TURBULENCE NEAR THE 100 KILOMETER LEVEL OF THE UPPER ATMOSPHERE

by C. G. Justus

TECHNICAL REPORT

Georgia Tech Project A652-001

Prepared for
National Aeronautics and Space Administration
Washington 25, D. C.

Contract No. NsG 304-63

November 1965

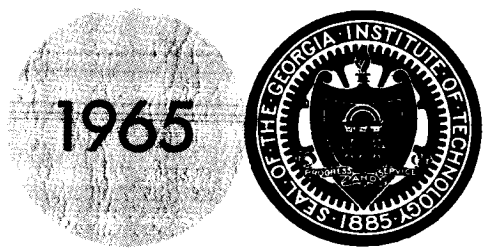

Engineering Experiment Station
GEORGIA INSTITUTE OF TECHNOLOGY
Atlanta, Georgia

TURBULENCE NEAR THE 100 KILOMETER LEVEL OF THE UPPER ATMOSPHERE

by

C. G. Justus

TECHNICAL REPORT*

Georgia Tech Project A652-001

Prepared for

National Aeronautics and Space Administration
Washington 25, D. C.

Contract No. NsG 304-63

November 1965

*Also submitted as a graduate thesis for the School of Physics, Georgia Institute of Technology.

ACKNOWLEDGMENTS

The author wishes to express his appreciation to Dr. Howard D. Edwards, of the School of Aerospace Engineering and formerly of the School of Physics, Georgia Institute of Technology, and the many people working with him both in the field and in the laboratory who, over a period of several years, have participated in the gathering and reduction of the wind data on which the analysis of this thesis is based. Without their enormous efforts this work would not have been possible. Thanks also go to Dr. R. G. Roper who provided both a copy of his thesis and enlightening discussion of some of the topics presented here. Funds for this work were provided by the National Aeronautics and Space Administration through grant NsG 304-63 and the United States Air Force through contract AF 19(628)-393.

TABLE OF CONTENTS

Table of Contents (Cont'd.)

LIST OF TABLES

LIST OF ILLUSTRATIONS

List of Illustrations (Cont'd.)

SUMMARY

Early investigators attributed many of the observed large scale irregularities in upper atmospheric winds to turbulence. Later, gravity wave theory was successful in explaining many of the properties of these large scale irregularities. This led some researchers to question whether turbulence existed at all as an ambient phenomenon of the upper atmosphere. One explanation of the observed small scale structure on chemical release clouds and meteor trails was that turbulence is produced by the rocket, release mechanism or meteor during its passage through the atmosphere. Comparison of the characteristics of turbulence observed from both meteor trails and chemical releases indicates that the turbulence must be a naturally occurring ambient phenomenon. This conclusion is also supported by the discrepancies between observed and predicted jet and wake turbulent velocities.

On chemical release clouds, many spherical protuberances or globules usually appear below a certain altitude. It is shown that the ambient turbulence provides an unstable medium in which small fluctuations in the release of chemical or meteoric material lead to the formation of these globules. The upper atmospheric turbulence has a rather sharp cutoff point, the turbopause, near 106 km, as determined by examination of the maximum altitude of globule formation on many chemical releases. Immediately below the turbopause the globules appear to be almost spherical, but they grow more fuzzy and ill-defined in appearance as the altitude decreases. This behavior is explained by the existence

and properties of a subrange of motion affected by buoyancy forces and acting only at small scales.

Turbulent winds determined by chemical release tracking are useful in obtaining estimates of the turbulent energy source parameter ϵ_s and the buoyancy and viscous dissipation terms ϵ_g and ϵ. In a stably stratified portion of the atmosphere, such as above the mesopause at about 85 km, all contribution to the energy source term ϵ_s must arise from wind shears. The buoyancy dissipation parameter ϵ_g is important only in such a stably stratified region. Turbulent diffusion of globules at times after release $t \gtrsim 200$ sec follows a $d^2 \sim \epsilon\, t^3$ law. The height variation of ϵ as determined from diffusive growth is in reasonable agreement with the turbulent wind determinations of ϵ. Both ϵ_s and ϵ_g are found to be slowly varying with altitude, having values of about 0.4 and 0.35 watts/kg respectively, in the height region from 90 km to the turbopause. However, ϵ increases rapidly with altitude. This observed rapid increase and the energy balance requirement $\epsilon < \epsilon_s$ indicate that turbulence cannot exist above 106 km, in agreement with observation. The observed height variation of ϵ is compatible with estimates of ϵ obtained at lower altitudes by other investigators.

During the time after release period $t \lesssim 150$ sec, the globules show a $d^2 \sim \epsilon_g\, t^5$ diffusion, indicating the presence of a buoyancy subrange affecting only the smaller scales. During the time after release interval $150 \lesssim t \lesssim 200$ sec, the buoyancy subrange no longer affects globule growth, and molecular diffusion, $d^2 \sim t$, alone accounts for the globule expansion during this period. The 150 second interval of buoyancy subrange diffusion is an appreciable fraction of the period $2\pi/\omega_g$ for

harmonic oscillation of a fluid element displaced from its equilibrium altitude in a stably stratified atmosphere. The 50 second period of molecular diffusion corresponds closely to the theoretically predicted time scale $\sqrt{2}/\omega_g$ of the largest buoyancy subrange eddies. The maximum buoyancy subrange size scale L_b varies with altitude but is approximately 0.8 km between the altitudes of 98 km and the turbopause. This value is predicted by the requirement that the characteristic buoyancy kinetic energy per unit mass $\frac{1}{2} v_b^2$ must be less than the observed turbulent kinetic energy per unit mass.

Suggested modifications are made for the form of the shear and energy spectrums of the turbulence. The experimental evidence supports the validity of these alterations and also allows evaluation of some of the constants which appear in the spectral law formulas. Both the spectrum functions and correlation techniques are used to determine the maximum scale L_o of the turbulent winds and the vertical scale of the total winds. The vertical scale of the total winds is found to vary approximately as the pressure scale height over a wide altitude region. The maximum vertical scale of the turbulent winds also varies with altitude, having a value of about 7 km at an altitude of 100 km. The maximum horizontal scale of the turbulent winds at 100 km is found to be about 10 km. Thus the strong vertical wind shears present introduce only a slight anisotropy into the turbulence.

The turbulent mixing length is found to be about 0.75 km below the turbopause and to be rapidly increasing above this altitude. Thus the mixing length and maximum buoyancy scale are approximately equal in the region immediately below the turbopause. The viscous cutoff size and

time scales L^* and τ^*, calculated theoretically, are not inconsistent with observation. However, these small scales cannot be observed with the resolution attainable with present data gathering techniques. Theoretical relations among the eddy scales L_o, L^* and the dissipation length L_d, previously derived for isotropic non-buoyancy turbulence, must be modified because of the important buoyancy effects present.

The characteristic time scale τ_o of the largest turbulent eddies is found to be 300 to 330 sec. Thus chemical cloud lifetimes of about 10 minutes allow ample time for observation of most, if not all of the turbulent spectrum. The observed value of τ_o is approximately equal to the period $2\pi/\omega_s$, where ω_s is the observed magnitude of the total wind shear.

The usual Richardson, Townsend and Layzer criteria for the onset of turbulence are examined and found to be unsuccessful in explaining the observed turbulence cutoff near 106 km. However, a generalized Richardson criterion is derived which does successfully predict turbulence only below 106 km. This generalized Richardson criterion is based on the energy requirement that the characteristic buoyancy kinetic energy per unit mass $\frac{1}{2} v_b^2$ must be less than the turbulent kinetic energy per unit mass which can be produced by wind shears.

The Reynolds criterion is also examined. It is found that this criterion will allow turbulence up to at most only a few kilometers above the observed 106 km turbopause. However, theoretical uncertainties as to the proper application of the Reynolds criterion in a free atmosphere may mean that the only restriction this criterion places on the turbulence is an absolute upper limiting altitude of 120 to 140 km.

CHAPTER I

ENERGY BALANCE

Introduction

In order to be characterized as turbulence, the motion field must satisfy certain requirements. It must be three dimensional, nonlinear, diffusive, rotational and dissipative, mechanical energy being transformed to internal energy through a cascade of eddies of diminishing size. The cascade, ending in viscous dissipation of energy from the smallest eddies, is connected with the nonlinearity, three dimensionality and rotationality of the field. The velocity components must be distributed irregularly and aperiodically in time and space.

The diffusive nature of turbulence is responsible for the transport of properties such as mass, momentum and heat. The transfer rate of the properties is, in general, greatly increased by the action of the turbulence. Time and length scales of the property-transporting motions are usually large compared to intermolecular dimensions and are often as large as the scales of the distribution of the transported properties. For this reason, turbulence is a continuum phenomenon.

The fact that turbulence is rotational, in the hydrodynamic sense of the word, does not mean that the motion of the eddies is actually one of rotation. In fact, such two dimensional rotating motions as vortex sheets and whirlpools are not to be considered turbulence, according to the above definition. An eddy is, instead, merely a portion of the fluid which moves more or less coherently with respect to the mean motion.

Alternatively, as a more mathematical description, an eddy may be considered as a component of the Fourier integral expansion of the velocity function. The expansion is usually made with respect to the wave number k. The associated eddy size ξ for wave number k is just $\xi = k^{-1}$.

Photographic tracking of chemical release clouds [Justus et al., 1964a, 1964b] provides information on the wind profile V(z) over a wide altitude range. The total winds are made up of prevailing, periodic tidal wave, gravity wave and turbulent components. Mean winds obtained from chemical release tracking provide averages over the cloud lifetime, which is typically five to 10 minutes. Frequently many protuberances in the form of nearly spherical globules appear on these clouds below about 106 km altitude. Individual tracking of these globules, or other identifiable cloud features, yields time varying winds. The intermediate time scale winds, v, are obtained by subtracting the average wind profile velocities from these time varying winds. Because of the relatively short lifetime of these clouds, large time scale gravity wave and/or turbulent components would be considered as part of the mean winds. However, results indicate that the "intermediate" scales of turbulence observable by chemical release tracking constitute most, if not all of the larger scales in the turbulent spectrum.

Several investigators have observed that above some altitude near 105 km molecular diffusion accounts for all of the chemical cloud expansion while below this altitude accelerated diffusion caused by turbulence takes place. Usually the globular structure of chemical releases exists only up to an altitude close to this transition point, the turbopause, where conditions change from turbulent to laminar. However, Cote [1965]

has pointed out that accelerated diffusion can be observed on sodium trails which have no globular structure.

There are three possible mechanisms for the production of the globular structure in chemical releases: (1) A reaction of the release vehicle or ejection mechanism creates the turbulence and the globular structure directly. (2) The turbulence is naturally occurring ambient turbulence and provides an unstable medium in which small fluctuations in the releasing of the chemical lead to globular structure of the cloud. (3) The turbulence is ambient in nature and provides the velocity fluctuations which produce the globules directly.

Comparison of the intensity and duration of the observed turbulence on chemical releases and meteor trails (see Appendix A) rules out the first of these. Cote's observations rule out the third and support the second mechanism. The cases in which globules are not produced in the turbulent zone are ones in which the cloud chemical was released at a very uniform rate or in a small concentration. The altitude at which globules cease to appear on a chemical release cloud is thus in most cases a good estimate of the turbopause altitude. Observations of the globule cutoff altitude on 21 chemical releases yielded an average value of 106 km ± 4 rms.

The globules appear to have an especially sharp edge on cesium clouds observed under twilight conditions by their infrared resonance radiation. However, globular structurc has been observed on several types of chemical clouds both at twilight and during the night. Chemical clouds with globular structure have an appearance similar to the globular structure of cumulus clouds or the mammilated under surface of

cumulonimbus or stratocumulus clouds in the lower atmosphere.

Although the chemical release globules depend on turbulent eddies for their existence, the globules themselves are not to be identified as eddies, since the globules are acted on by the eddies and expand by turbulent diffusion.

Even on clouds where the globules appear sharpest, they become generally smaller with decreasing altitude and in the vicinity of 90 km cease to have their customary near spherical shape. Below this altitude the clouds appear generally fuzzy but have no spherical globular structure.

Definitions of the Energy Balance Terms

Since turbulence is dissipative, statistically steady turbulent motion requires the existence of a continuous external energy source. If the air is thermally unstable, the potential energy of the unstable arrangement can supply the energy for turbulence. In a stably stratified region of the atmosphere, such as above the mesopause at about 85 km, wind shears provide the only source of energy for maintaining turbulence. Stable stratification also makes it possible for energy to be dissipated from the air motions by the effects of buoyancy forces.

For statistically stable turbulence in a stably stratified medium, the energy balance equation for the turbulent kinetic energy per unit mass may be written

$$\epsilon_s = \epsilon_g + \epsilon \quad , \tag{1}$$

where ϵ_s is the rate per unit mass at which kinetic energy is being supplied to the turbulence by wind shears, and ϵ_g and ϵ are the rates per unit mass at which kinetic energy is being dissipated by buoyancy and

viscous forces, respectively.

Townsend [1957] gives the relations

$$\epsilon_s = \sum_{i,j} \overline{v_i v_j} \frac{\partial V_i}{\partial x_j} \quad , \tag{2}$$

and

$$\epsilon_g = \sum \frac{g_i}{T} \overline{\theta v_i} = \frac{g}{T} \overline{\theta v_z} \quad , \tag{3}$$

where g is the acceleration of gravity, T is the mean temperature and θ is the fluctuation in temperature. The temperature fluctuation is the difference between the temperature of a fluid element and the mean temperature at the altitude of the element. If a fluid element, initially in temperature equilibrium at a height z, is displaced adiabatically to the altitude $z + \zeta$, and assumes the ambient pressure, the temperature fluctuation is given by

$$\theta = T(z + \zeta) - T(z) = \left(\frac{\partial T}{\partial z} + \frac{g}{C_p} \right) \zeta \quad , \tag{4}$$

where C_p is the specific heat at constant pressure. For an ideal gas g/C_p is equivalent to $\left(\frac{\gamma - 1}{\gamma} \right) (Mg/R)$, where γ is the ratio of specific heats, M is the molecular weight and R is the universal gas constant. For the altitudes of interest here either expression may be used without appreciably altering the calculations. The parameter ω_g, defined by

$$\omega_g^2 = \frac{g}{T} \left(\frac{\partial T}{\partial z} + \frac{g}{C_p} \right) \quad , \tag{5}$$

has units of inverse time and is the frequency of harmonic oscillation [Nawrocki and Papa, 1963] which a fluid element would experience after a small displacement from its equilibrium altitude.

When a fluid element leaves the level z and carries momentum to the level $z + \zeta$, a fluctuation in velocity of magnitude v is produced. This horizontal turbulent velocity would be given by

$$v_x = V_x(z + \zeta) - V_x(z) \approx \zeta \frac{\partial V_x}{\partial z} \quad . \tag{6}$$

Therefore the use of (5) and (6) in equation (3) produces an approximate relation for ϵ_g given by

$$\epsilon_g = \omega_g^2 \frac{\overline{v_x v_z}}{\left(\frac{\partial V_x}{\partial z}\right)} \quad . \tag{7}$$

Lamb [1945] gives a relation for ϵ in a viscous compressible fluid, which can be put in the form

$$\epsilon = 2\eta \sum_i \overline{\left(\frac{\partial v_i}{\partial x_i}\right)^2} + \eta \sum_{cyc} \overline{\left(\frac{\partial v_z}{\partial y} + \frac{\partial v_y}{\partial z}\right)^2} - \frac{2\eta}{3} \left(\sum_i \overline{\frac{\partial v_i}{\partial x_i}} \right)^2 \quad , \tag{8}$$

where η is the kinematic viscosity and $\sum_{cyc}$ indicates a sum over the full cyclic range of components. For an incompressible fluid the last term in (8) would be identically zero. If the turbulence is also isotropic, it can be shown [Taylor, 1935] that (8) reduces to

$$\epsilon = 6\eta \left[\overline{\left(\frac{\partial v_x}{\partial x}\right)^2} + \overline{\left(\frac{\partial v_x}{\partial y}\right)^2} + \overline{\frac{\partial v_y}{\partial x} \frac{\partial v_x}{\partial y}} \right] \quad , \tag{9}$$

which can be further reduced to

$$\epsilon = \frac{15\eta}{2} \overline{\left(\frac{\partial v_x}{\partial y}\right)^2} \quad . \tag{10}$$

Turbulent Diffusion

Cote [1962, 1965] has summarized several theories of turbulent diffusion. Several relations he discusses can be put in the form

$$d^2 \sim v_o^{6-2n} \epsilon^{n-2} t^n \quad , \tag{11}$$

where d is the diameter of the diffusing cloud at time t after its injection and v_o is the rms turbulent velocity. The exponent n in (11) can take on the values 2,3,4 or 6 depending on the form assumed for the turbulent energy spectrum or on other assumptions about the nature of the turbulence. Note that n = 3 in (11) eliminates the dependence on v_o. There are at least three theories which predict t^3 dependence in (11). One due to Batchelor [1950] is based on Kolmogoroff's similarity principle and predicts the specific form

$$d^2 = \frac{16}{3} \epsilon t^3 \quad . \tag{12}$$

Lin's theory [1960] of turbulent diffusion predicts

$$d^2 = \frac{4}{3} B t^3 \quad , \tag{13}$$

where B is a parameter which Lin proposes to be proportional to ϵ through some universal function of the Reynolds number. Tchen's theory [1961] of diffusion in turbulent shear flow predicts $d^2 \sim t^2$ for high shear fields

and $d^2 \sim t^3$ for low shear fields. Tchen's predictions for diffusion in shear turbulence are based on his earlier derivations [Tchen, 1954] for the energy spectrum E(k), to be discussed in Chapter II. The predicted form for E(k) depends on the magnitude of the shear $V' = \frac{\partial V_i}{\partial x_j}$, and the expected diffusion law depends on the form of E(k). For large V', the predicted forms are $E(k) \sim V'k^{-1}$ and $d^2 \sim t^2$. For small V', the spectral and diffusion law forms become $E(k) \sim k^{-5/3}$ and $d^2 \sim t^3$.

The diffusion theories of Batchelor, Lin and Tchen do not take into account the effects of buoyancy. Bolgiano [1959] has suggested that the necessity for including ϵ_g in the energy balance equation for a stably stratified portion of the atmosphere leads to alterations in the energy spectrum E(k). The expression for ϵ_g, given by equation (3), contains the covariance $\overline{\theta v_z}$ of the temperature fluctuation and the vertical turbulent velocity. A positive value for this covariance indicates that turbulent kinetic energy is being converted to potential energy by the buoyancy effects associated with the turbulence working against gravity. Bolgiano suggests that if the Reynolds number (see Chapter I) is sufficiently large there will be a subrange of wave numbers k over which this covariance remains positive. This energy extraction in the buoyancy subrange means that the viscous dissipation ϵ may be significantly less than the rate of generation of turbulent kinetic energy ϵ_s. The difference in these terms is ϵ_g, the work done against buoyancy.

Bolgiano suggests that the importance of this energy extraction by the buoyancy effects means that ϵ_g and ω_g are the important parameters which determine E(k) in the buoyancy subrange. He predicts the form $E(k) \sim k^{-11/5}$ in this subrange. This alteration in E(k) in the buoyancy subrange

should lead to an associated alteration of the diffusion law. Assuming that the parameters ϵ_g and ω_g also determine the diffusion law in the buoyancy subrange, Bolgiano derived a t^5 law for this subrange which is given by

$$d^2 = \beta \omega_g^2 \epsilon_g t^5 \quad , \tag{14}$$

where the dimensionless constant β is of order unity.

Therefore if observations of actual turbulent diffusion yield a time exponent compatible with (11), ϵ can be calculated. However, if a t^5 diffusion is observed, this would indicate the existence of a buoyancy subrange with the diffusion law being independent of ϵ .

Experimental Evaluation of the Energy Balance Terms

The turbulent winds v, determined as outlined in the introduction, may be used in (2) and (7) to determine ϵ_s and ϵ_g. The strong vertical shear components $\frac{\partial V_x}{\partial z}$ and $\frac{\partial V_y}{\partial z}$ for a given set of wind data are easily determined from the wind profile. The horizontal shear components are taken to be about 0.05 m/sec/km as indicated by velocity differences obtained from chemical trails separated by several tens of kilometers [cf. Rosenberg and Justus, 1965]. Values of ω_g may be calculated from 1962 U. S. Standard Atmosphere data. By approximating derivatives with ratios of finite differences, one may also use the turbulent winds in (8), (9) and (10) to calculate ϵ, again using 1962 U. S. Standard Atmosphere data to calculate η . The formula used for this purpose is

$$\eta = \frac{1.458 \times 10^{-6} \, T^{3/2}}{\rho \, (T + 110.4)} \ (m^2/sec) \quad , \tag{15}$$

where T and ρ are the atmospheric temperature and density in ^{o}K and kg/m^3. Relation (15) yields an unknown amount of uncertainty in η, but it must be used since tabulated values are not given above 90 km.

Turbulent wind data from several chemical releases have been analyzed and, although there is a fairly large scatter in the data points, an exponential function represents the height variation of ϵ very well for each of the three cases (8), (9) and (10). Roper [1963] has reported a rather large seasonal variation in ϵ as determined from meteor trail investigation. Undoubtedly there is some seasonal variation as well as diurnal and even small scale spatial variation in ϵ . This could be responsible for much of the scatter in the calculated ϵ values obtained from the chemical release data. However, there is not a sufficient amount of these data for analysis of the variations to have any statistical significance. An exponential function fit to all of the observed data would thus represent an appropriate average over the different seasons, times of day and spatial locations from which the data were obtained. Figure 1 shows the exponential functions obtained by a least squares fit of the ϵ data calculated from equations (8), (9) and (10). Each curve shows ϵ to be increasing more rapidly than the kinematic viscosity η, which is also shown in Figure 1 for reference.

Globule sizes versus time have been measured for several chemical releases launched at both morning and evening twilight. Globules that can be observed early in their lifetimes show an unusual growth behavior. Figure 2 shows an example of the globule growth curves obtained. The case illustrated is a cesium globule at 97.7 km. The general behavior of globules exhibiting the anomalous early growth is a very rapid expansion

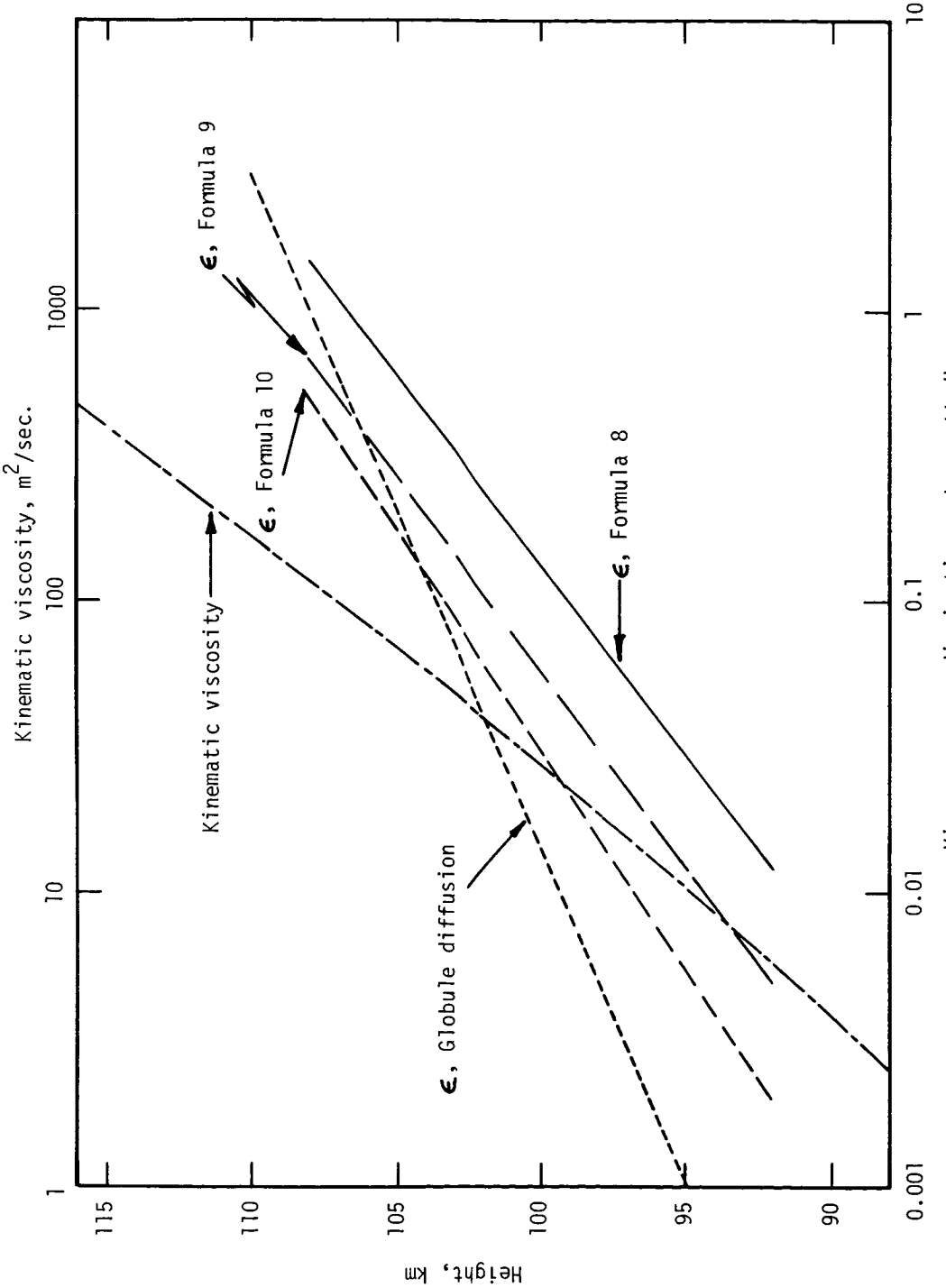

Figure 1. Viscous Dissipation Parameter ε and the Kinematic Vuscosity η versus Altitude.

during the first 150 ± 40 seconds after release, followed by a period of almost no growth which lasts for 50 ± 10 seconds. After the period of slow growth, called the level phase, the globule expansion rate increases but the growth does not proceed as rapidly as during times before the level phase. Although apparent anomalies in globule growth could be produced by changing sky background or changing camera f/stops, the observed level phase is apparently a real effect. This is borne out by the consistent height variation of the diameter at which the globule growth levels off, as illustrated in Figure 3. This graph shows that the diameter attained at the time of the level phase is nearly constant between 98 and 106 km but undergoes a fairly rapid variation below and above these altitudes.

For comparison with turbulent diffusion formulas, the growth curves are best plotted in the log-log form shown in Figure 4, which shows the same growth curve illustrated in Figure 2. Figure 4 shows an initial expansion according to $d^2 \sim t^{7 \pm 2}$. As determined from all globules observed, the average initial growth follows a $d^2 \sim t^{5 \pm 1}$ expansion, indicating that the initial growth is due to the effect of a buoyancy subrange. The average observed constant of proportionality for $d^2 \sim t^5$ diffusion is 0.6×10^{-4} m^2/sec^5. However, measurement inaccuracies at small globule diameters mean that this value is probably accurate only to within about a factor of three. For the 90 to 105 km range, equation (7) yields approximately 0.35 watts/kg for ϵ_g and ω_g^2 is about 6×10^{-4} sec^{-2} in this height interval. Therefore the observed globule growth in the early phase is

$$d^2 = 0.3 \, \omega_g^2 \, \epsilon_g \, t^5 \quad , \tag{16}$$

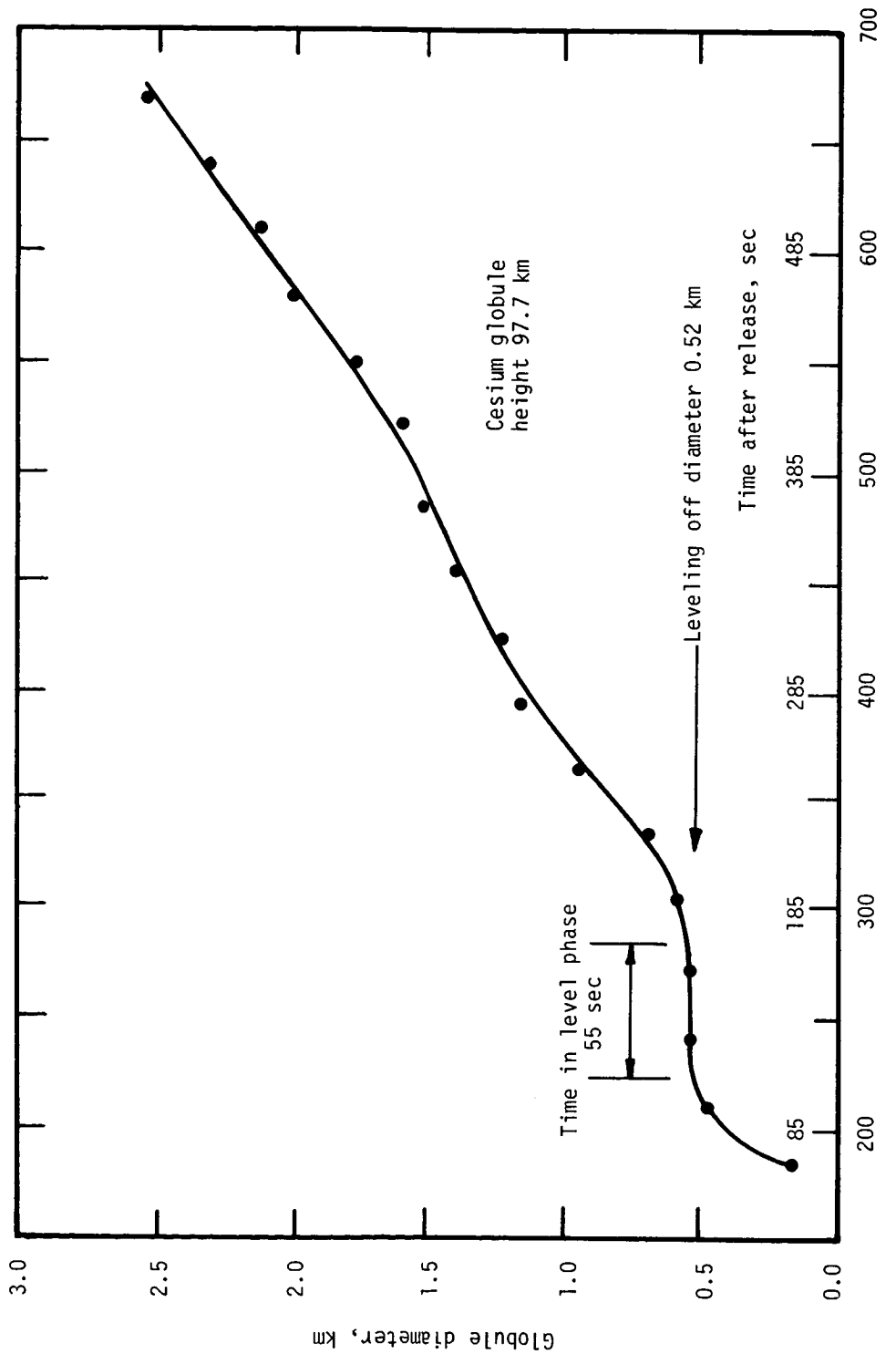

Figure 2. Sample Globule Growth Curve - Diameter versus Time after Rocket Launch.

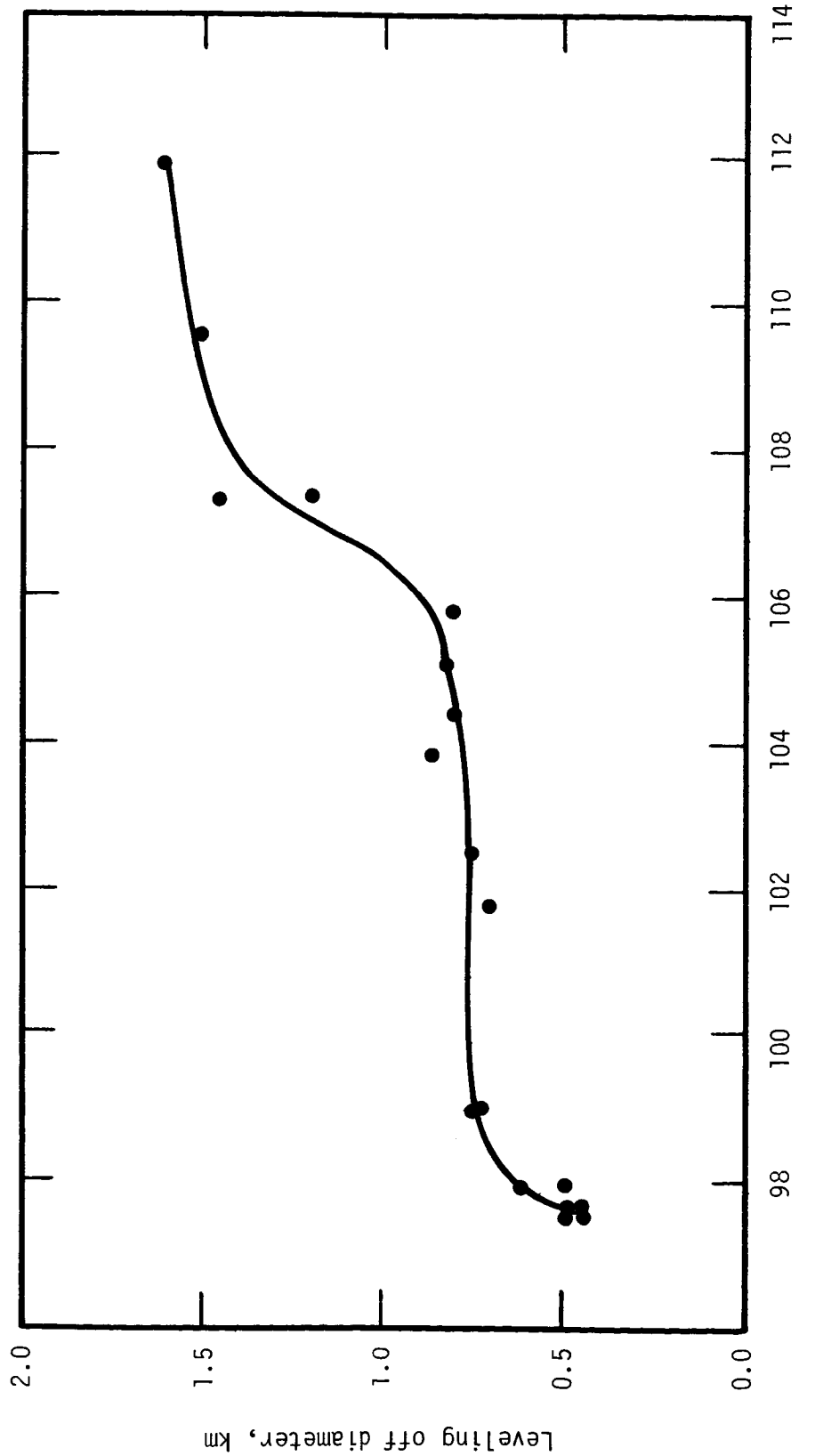

Figure 3. Height Variation of the Globule Leveling off Diameter.

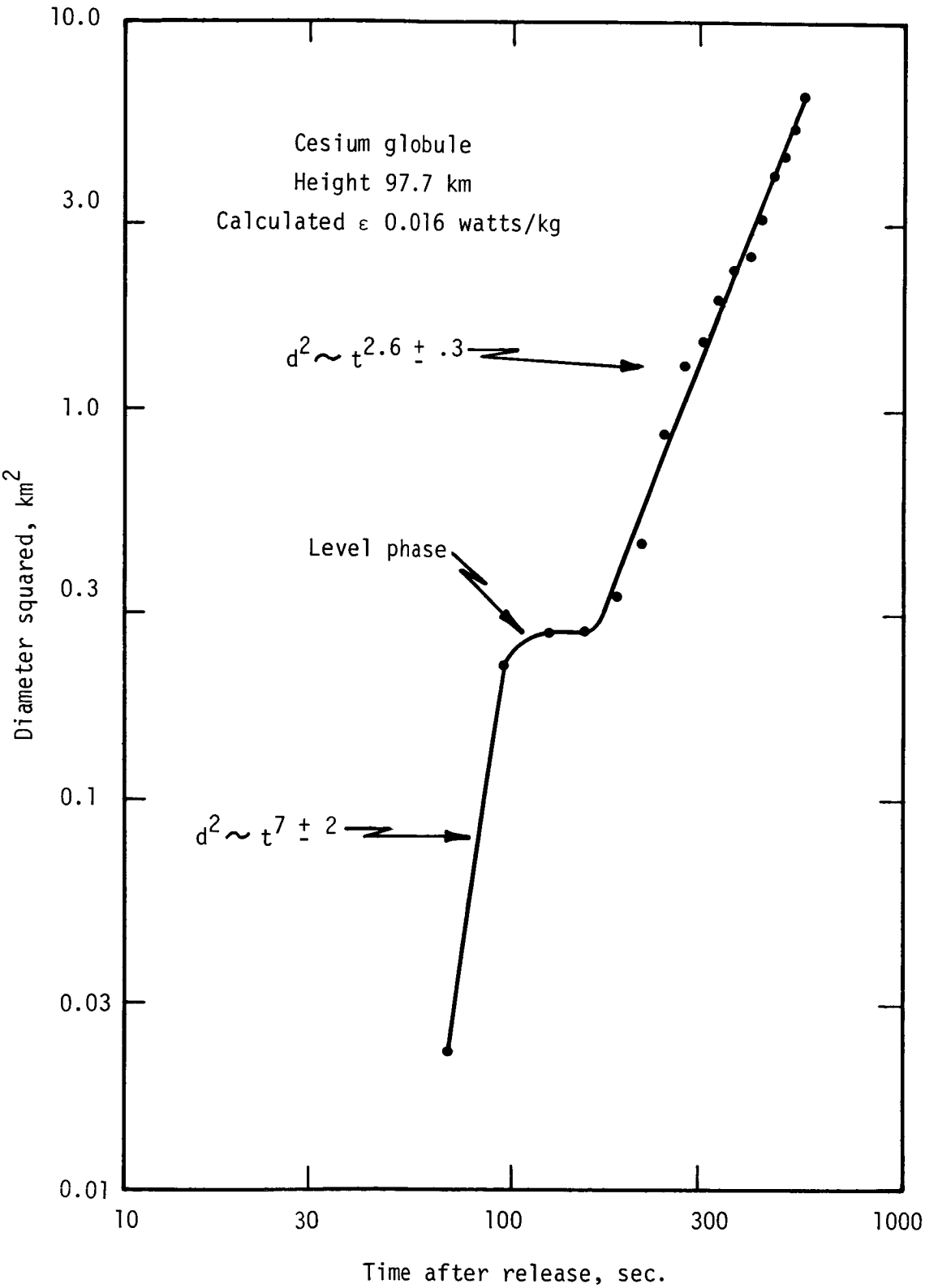

Figure 4. Globule Growth of Figure 2, on log-log Scale.

with a probable error of a factor of three in the numerical constant. This is better than mere qualitative agreement with the t^5 diffusion equation (14) for a buoyancy subrange. The t^5 growth occurs only at small globule sizes because energy balance considerations limit the buoyancy subrange to small globule scales. This limitation of the buoyancy subrange to small scales will be discussed more fully in Chapter III which deals with scale sizes.

Figure 3 shows that the maximum size scale affected by the buoyancy subrange is decreasing with decreasing altitude. This accounts for the spherical shape of the globules in the 90 to 106 km region and the more fuzzy appearance of the clouds below 90 km. The motions in the buoyancy subrange are somewhat more ordered than those in the larger scale range. In the 90 to 106 km region the buoyancy subrange can affect the cloud structure during a comparatively long period of its initial growth and can shape the cloud into regular spherical globules. At lower altitudes the buoyancy subrange cannot act on the cloud elements for a sufficient length of time to form spherical globules and the motions of scales larger than the buoyancy subrange break up the cloud into a fuzzy appearance.

When the t^5 growth becomes inoperative the small growth during the level phase can be accounted for by molecular diffusion alone. For the globule growth shown in Figure 4 the value of d^2 at the cessation of the t^5 expansion is 2.2×10^5 m^2. At the end of the level phase the value of d^2 is 2.9×10^5 m^2. Since for this globule the level phase lasts about 55 seconds, the observed growth during this period would be accounted for by a molecular diffusion coefficient of $D = \frac{\Delta d^2}{8\Delta t} \approx 2 \times 10^2$ m^2/sec, a

reasonable value for cesium at 98 km.

Since molecular diffusion is important during the level phase growth, the sharpness of cesium globules compared to those on other chemical clouds may be due to the fact that cesium, the heaviest cloud material used, has the smallest molecular diffusion coefficient. However, cesium must be observed at twilight by its resonance radiation, and the sharpness of the globules may be merely a function of the optical density of the released cloud material.

After the end of the level phase, globules again undergo an accelerated power law diffusion. For the globule growth shown in Figure 4 the expansion follows $d^2 \sim t^{2.6 \pm 0.3}$. Since the exponent is close to three, the power law for globule growth in this phase was determined by least squares analysis using the formula

$$d^2 = \frac{16}{3} \epsilon^{n-2} t^n \quad , \tag{17}$$

which allows determination of n and ϵ . The numerical factor in (17) is taken from (12), since none of the other turbulent diffusion formulas predicts a specific value for this constant. This "constant" may even vary with altitude if (13) is applicable, since the Reynolds number varies with altitude. The average value of the exponent n obtained from many globule observations is 3.0 ± 0.4 rms. Figure 1 shows the best least squares exponential curve which fits the height variation of ϵ determined from the globule diffusion. Although this method of determining ϵ is independent of the calculated values of η , this graph also shows a rapid increase of ϵ with altitude.

From measurements of diffusive growth of turbulent trails Cote [1965] observes a $d^2 \sim t^2$ expansion, in disagreement with the globule diffusion $d^2 \sim t^3$ reported here. However, Cote points out that difficulties in accounting for changing sky background make it impossible for his observations to completely rule out $d^2 \sim t^3$ diffusion. Cote's observations are dependent on sky background because they rely on densitometric determination from the cloud image on film of the shape of the profile of cloud light emission above that of background. The same sky background difficulties would admittedly plague the globule measurements reported here, but, since $d^2 \sim t^3$ globule diffusion has been observed against both increasing and decreasing sky background, the effects of sky background change seem to be minor. Globule expansion can rarely be measured beyond diameters of about three km. Therefore an alternate method, independent of sky background, for measuring large scale diffusion effects would be most helpful in determining if Cote's $d^2 \sim t^2$ result indicates a transition to a different diffusion law at large scales (as might be expected from Tchen's theory) or is merely an effect of sky background. One possible method for studying large scale turbulent diffusion would be by observing the growth with time of the separation distance between pairs of globules at approximately the same altitude. These measurements would be independent of sky background.

Although the agreement between the several estimates of ϵ shown in Figure 1 seems to be embarassingly poor, Figure 5 shows that it is actually much better than the agreement between estimates of ϵ obtained by various investigators at lower altitudes. This figure shows a summary by Lettau [1961] of values of ϵ obtained from diffusion and wind profile observations

in the altitude range from one cm to 40 km. The uncertainty in ϵ is as much as three orders of magnitude at some of these lower altitudes. This fact plus the uncertainties in η and the numerical constant in (17) makes the agreement in the graphs of Figure 1 seem good indeed. Figure 5 also shows the variation of the average ϵ determined from the chemical release data. The observed height variation between 90 and 110 km fits well with the lower altitude data, under the assumption that ϵ continues to decrease with decreasing altitude, diminishing by approximately an additional three orders of magnitude from 90 to 30 km.

The average ϵ obtained from the four curves in Figure 1 is plotted in Figure 6. This figure also shows the exponential curves fit by least squares to the data points for ϵ_s and ϵ_g obtained from formulas (2) and (7). Due to scatter in the ϵ_s and ϵ_g data points, these curves are probably accurate only to within about a factor of two. To within this limit of accuracy $\epsilon_s = \epsilon_g + \epsilon$ holds for the curves shown over the height range from 92 to 106 km. The ϵ curve intersects the ϵ_s curve at 106 km and because ϵ continues to increase rapidly, the energy balance requirement $\epsilon < \epsilon_s$ means that turbulence cannot be maintained above this altitude. This 106 km intersection agrees well with the average observed cutoff altitude for globule formation. The observed region below 98 km where $\epsilon_g > \epsilon_s$ is also physically impossible if turbulence is to exist there, but this discrepancy can easily be accounted for within the possible errors in the ϵ_s and ϵ_g curves.

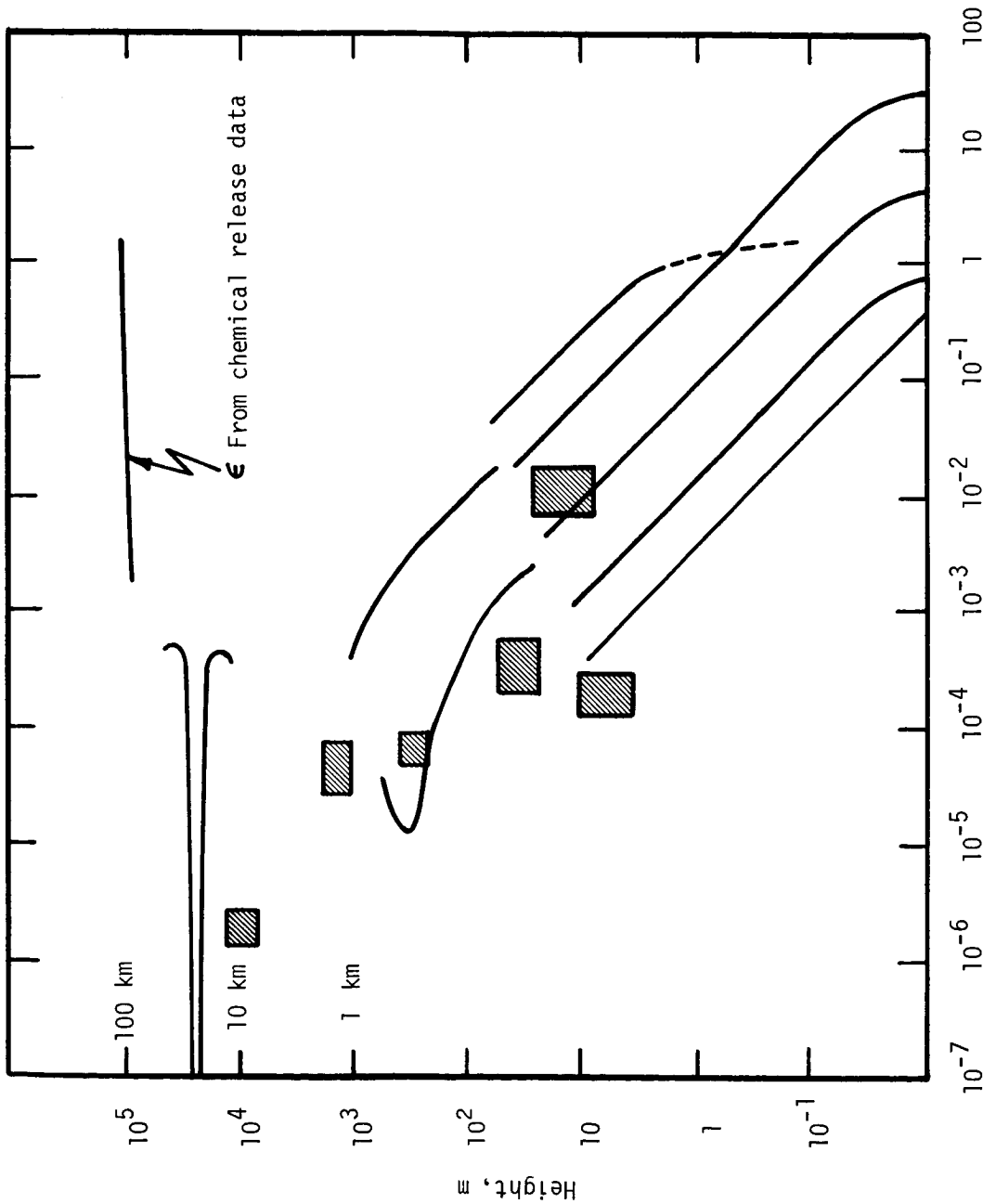

Figure 5. Summary of Viscous Energy Dissipation Rate Determinations from Altitudes of One cm to 110 km.

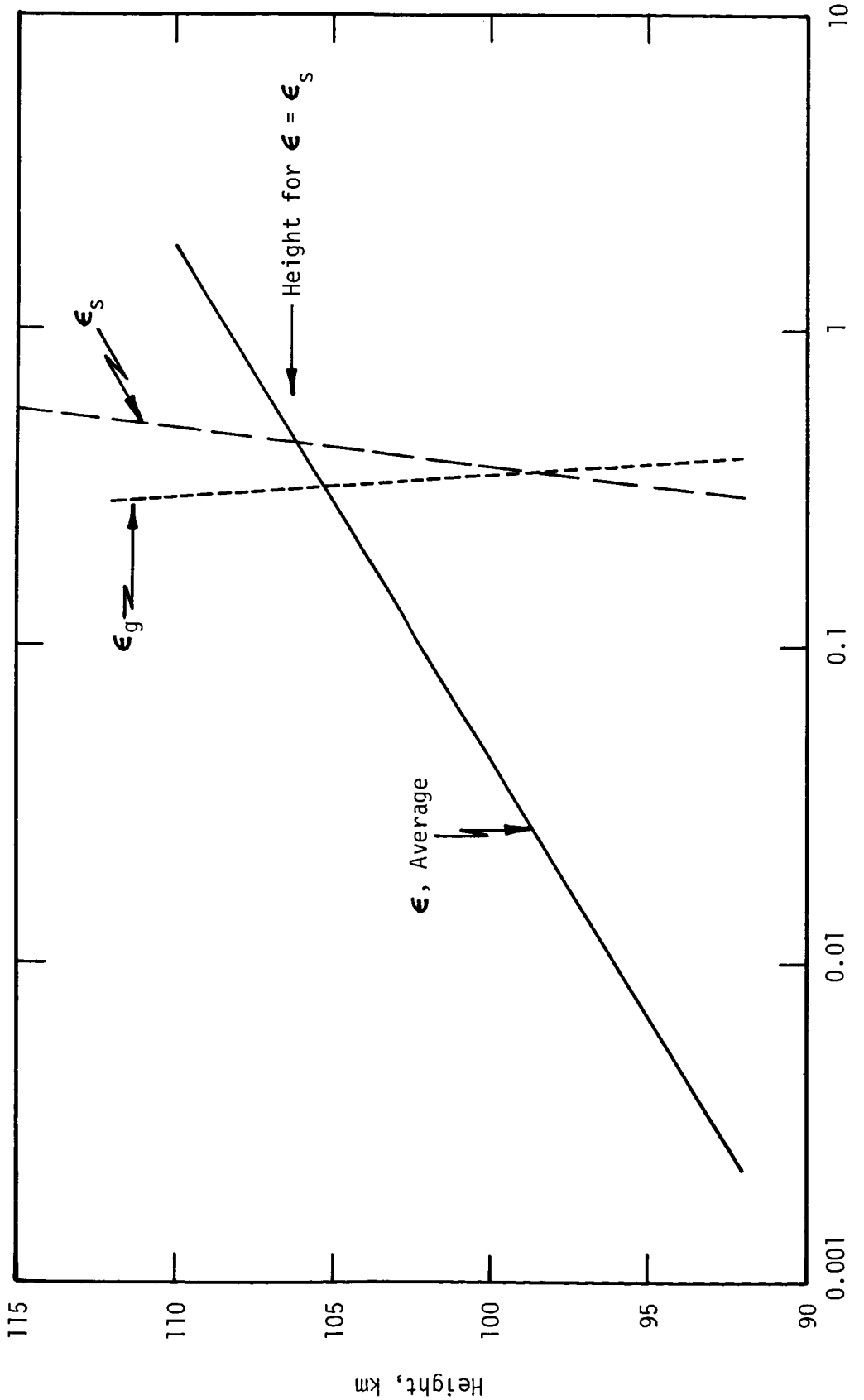

Figure 6. Height Variation of the Three Energy Balance Parameters.

CHAPTER II

SHEAR AND ENERGY SPECTRUMS

Previous Energy Spectrum Theories

According to the theory of homogeneous turbulence developed by Kolmogoroff [1941 a, 1941 b] the turbulent field may be characterized by three scale ranges. For eddy scale ξ the three scale ranges, in terms of $k = \xi^{-1}$, are: (1) the large scale fluctuations $0 \leq k \leq k_o$, which carry the turbulent energy extracted from the mean flow at a rate per unit mass ϵ_s, (2) the isotropic inertial subrange which has random statistical properties and transfers energy from larger to smaller scales with negligible energy loss and (3) the viscous dissipation region $k^* \leq k < \infty$ where the kinetic energy of the smaller eddies is dissipated by viscous forces at a rate per unit mass ϵ. Since no buoyancy forces are present in this theory, the energy balance equation is just $\epsilon_s = \epsilon$. Figure 7(a) shows schematically the energy spectrum $E(k)$, the energy per unit mass for wave numbers between k and $k + dk$. In the inertial subregion E is a function of ϵ and k according to the Kolmogoroff theory.

Bolgiano [1959] has proposed a theory which accounts for buoyancy effects and divides the energy spectrum into four subranges as shown in Figure 7(b). The large scale range $0 \leq k \leq k_o$ and the viscous dissipation range $k^* \leq k < \infty$ remain as before. The region between k_o and k^* is divided into a buoyancy subrange $k_o \leq k \leq k_B$ in which $E = E(\epsilon_g, k)$ and the usual inertial subrange only in the range $k_B \leq k \leq k^*$ in which $E = E(\epsilon, k)$. The energy balancy equation is $\epsilon_s = \epsilon_g + \epsilon$, where ϵ_g is the rate per unit

mass at which kinetic energy is removed from the turbulence by the buoyancy action.

The results of Chapter I, however, indicate that the buoyancy subrange affects only the small scale (hence large k) sizes, and that turbulence is observed at larger scales (smaller k) than those affected by buoyancy. Hence the actual energy spectrum must be something like the one shown schematically in Figure 7(c), with the inertial subrange in the region $k_o \leq k \leq k_b$ and the buoyancy subrange in the region $k_b \leq k \leq k^*$. Experimental determination of the smallest buoyancy scale k_B shows it to be approximately equal to k^*. It is an energy balance requirement which demands the upper scale cutoff of the buoyancy subrange, as will be discussed in the following chapter. Data are presented in this chapter which support the assumption that $E = E(\epsilon_s, k)$ in the inertial subrange and $E = E(\epsilon_g, k)$ in the buoyancy subrange with $E(\epsilon_g, k)$ being the form predicted by Bolgiano and $E(\epsilon_s, k)$ coming from existing non-buoyancy theories but obtained by substitution of ϵ_s for ϵ in the functions $E(\epsilon, k)$ which they predict.

Definitions of the Spectrum Functions

The spectrum theories discussed in the previous section are actually applicable only for non-shear turbulence or for turbulence in which wind shears do not impose a significant anisotropy on the motion field. As mentioned in Chapter I, there are strong vertical shears $\frac{\partial V_x}{\partial z}$ and $\frac{\partial V_y}{\partial z}$, but the horizontal shears are small in magnitude. Thus the turbulence in the upper atmosphere could be anisotropic in the vertical direction. Evidence presented later in this chapter indicates, however, that these shears do not introduce a drastic anisotropy. Therefore it seems reasonable that the concepts of division of the energy spectrum into the subranges

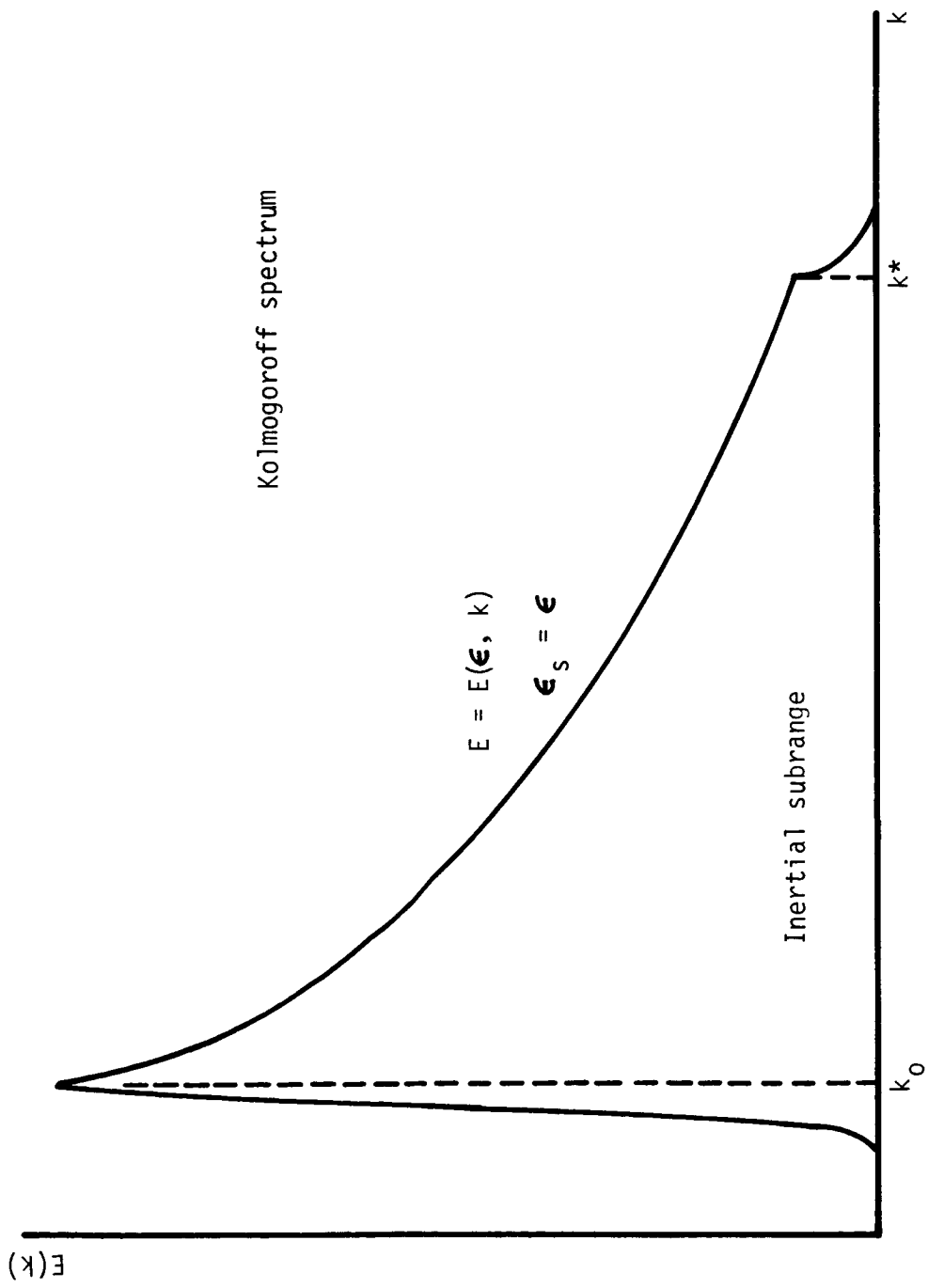

Figure 7a. Schematic Graph of the Energy Spectrum Function for Kolmogoroff Type Homogeneous Turbulence.

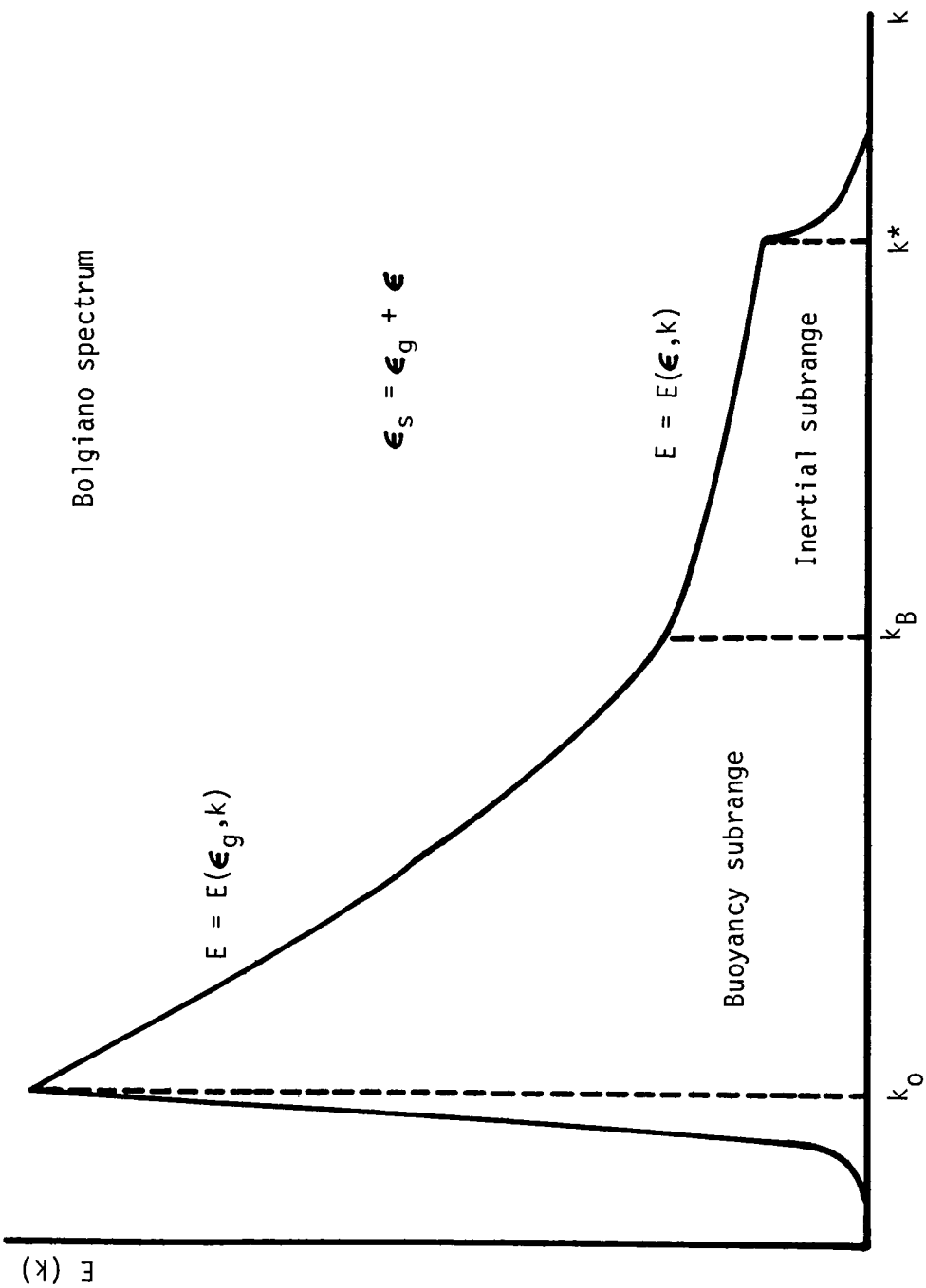

Figure 7b. Schematic Graph of the Energy Spectrum Function for Bolgiano Type Buoyancy Turbulence.

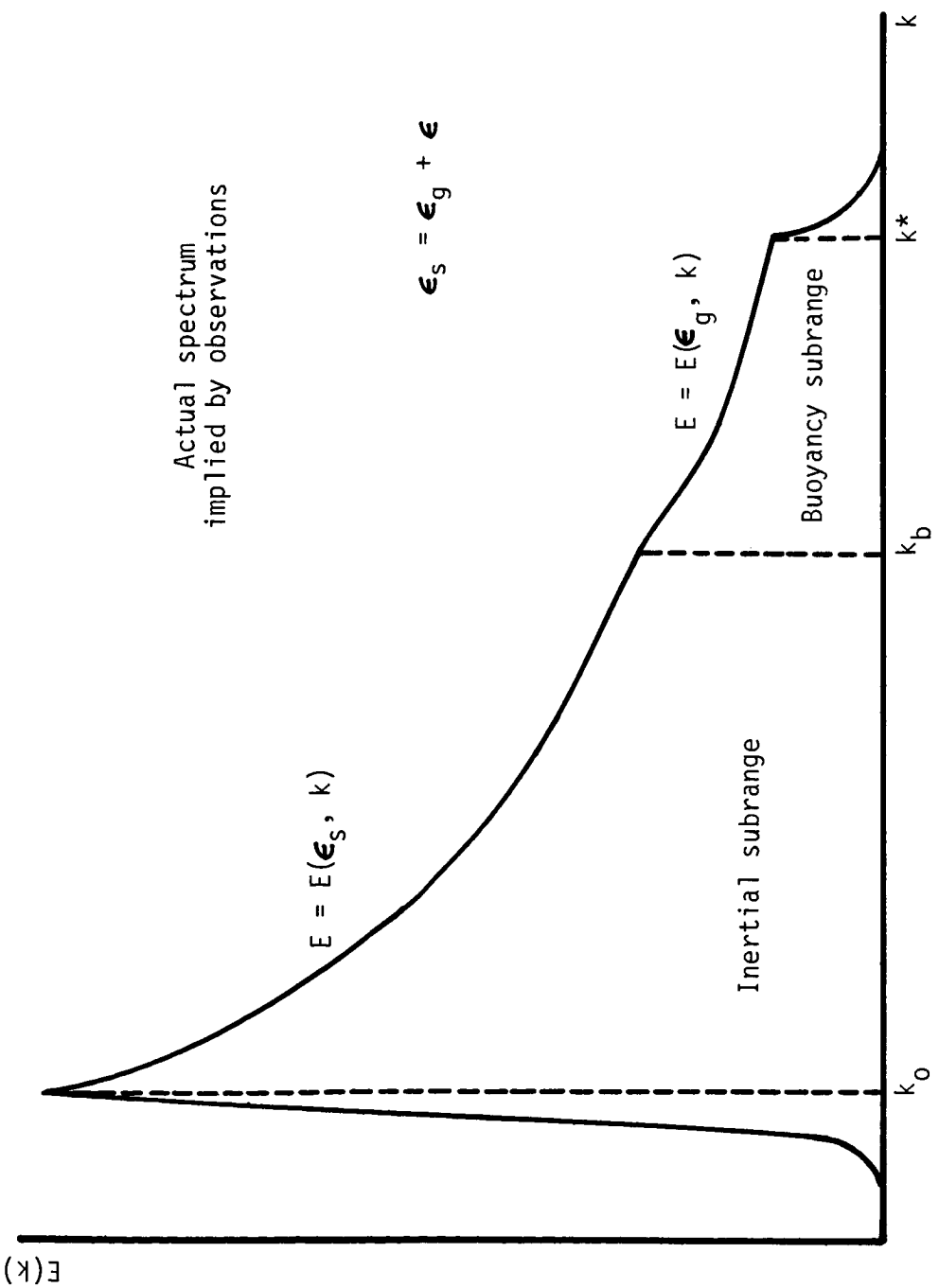

Figure 7c. Schematic Graph of the Energy Spectrum Function for the Observed Turbulence.

shown in Figure 7(c) is reasonable, but that the actual form of the energy spectrum E(k) should come from shear turbulence theory. Tchen [1954, 1961] has formulated such a theory.

Two important spectrums describing turbulent shear flow are the energy spectrum E(k), previously defined, and the shear spectrum F(k), which has a similar definition with respect to the shear across eddies of wave number between k and k + dk. Both E(k) and F(k) have dimensions of $(\text{length})^3/(\text{time})^2$.

If one uses Tchen's theory and substitutes ϵ_s for ϵ, the spectrums E(k) and F(k) for low shear fields in the inertial subrange of shear turbulence are given by

$$E(k) = \alpha\, \epsilon_s^{2/3}\, k^{-5/3} \tag{18}$$

and

$$F(k) = \beta\, \epsilon_s^{1/3}\, k^{-7/3} \quad , \tag{19}$$

where α is a dimensionless constant of order unity and β is a parameter which depends on the mean flow and has units of frequency (or shear).

Equation (18) is the same form predicted by Kolmogoroff's theory, except for the fact that $\epsilon = \epsilon_s$ in that theory but $\epsilon \neq \epsilon_s$ for shear turbulence with buoyancy effects. Relation (18) is also justified by the fact that Tchen's theory for low shear fields predicts the $d^2 \sim t^3$ diffusion observed from globule expansion.

For upper atmospheric turbulence it is difficult to measure the spectrums E(k) and F(k) directly. However, the methods developed by Blamont and de Jager [1961] and extended by Zimmerman [1962] allow infor-

mation about the spectrums to be obtained from the spectrum functions $\overline{E}(k)$ and $\overline{F}(k)$, defined by

$$\overline{E}(k) = \int_k^\infty E(k)\, dk \tag{20}$$

and

$$\overline{F}(k) = \int_k^\infty F(k)\, dk \quad . \tag{21}$$

These are essentially the spectrums E and F averaged over all eddy scales up to $\xi = k^{-1}$. Neglecting the effects of the change in E(k) for $k > k_b$, one may substitute (18) and (19) into (20) and (21), obtaining

$$\overline{E}(k) = \alpha\, \epsilon_s^{2/3} \int_k^\infty k^{-5/3}\, dk = \frac{3}{2}\, \alpha\, \epsilon_s^{2/3}\, k^{-2/3} \tag{22}$$

and

$$\overline{F}(k) = \beta\, \epsilon_s^{1/3} \int_k^\infty k^{-7/3}\, dk = \frac{3}{4}\, \beta\, \epsilon_s^{1/3}\, k^{-4/3} \quad . \tag{23}$$

In terms of the eddy scale ξ, these relations would be

$$\overline{E}(\xi) = \frac{3}{2}\, \alpha\, \epsilon_s^{2/3}\, \xi^{2/3} \tag{24}$$

and

$$\overline{F}(\xi) = \frac{3}{4}\, \beta\, \epsilon_s^{1/3}\, \xi^{4/3} \quad . \tag{25}$$

Experimentally, the functions $\overline{E}$ and $\overline{F}$ may be evaluated by averages

over the velocity field. The observed spectrum functions $\overline{E}_o$ and $\overline{F}_o$ are

$$\overline{F}_o(\xi) = \left\langle [v(z) - v(z + \xi)]^2 \right\rangle \tag{26}$$

and

$$\overline{E}_o(\xi) = \tfrac{1}{2}\left\langle \left| v^2(z) - v^2(z + \xi) \right| \right\rangle , \tag{27}$$

where the averages are taken over some range of altitude z.

Another spectrum function of importance is the motion spectrum function, which comes from homogeneous non-shear turbulence theory and is defined similarly to (26) by the relation

$$f(\delta) = \left\langle [v(\underline{r}) - v(\underline{r} + \underline{\delta})]^2 \right\rangle , \tag{28}$$

where the average is taken over the vector position $\underline{r}$, $\underline{\delta}$ is a vector displacement from $\underline{r}$, and δ is the magnitude of the vector $\underline{\delta}$. Batchelor [1947] has shown that this function is given by

$$f(\delta) = \gamma\, \epsilon_s^{2/3}\, \delta^{2/3} \left(1 + \frac{\delta_1^2}{3\delta^2} \right) \approx \gamma\, \epsilon_s^{2/3}\, \delta^{2/3} , \tag{29}$$

where γ is a dimensionless constant of order unity and δ_1 is the component of $\underline{\delta}$ in the direction of the turbulent wind component v. Again ϵ_s has been substituted for ϵ in the original formulas, but for homogeneous non-shear turbulence with no buoyancy, to which the original theory applies, $\epsilon_s = \epsilon$. Experimental evidence presented in the following sections justifies the use of ϵ_s in (29) and the other spectrum functions.

Experimental Evaluation of the Spectrum Functions

Photographic tracking of chemical trails provides information on the wind profile over an extensive altitude range. The total wind profile contains prevailing, periodic tidal wave and gravity wave winds, called collectively the mean winds, plus the small and possibly large scale turbulent components. An attempt to eliminate the mean winds can be made by subtracting an arbitrary function of altitude, resulting in a profile of residual winds.

Total wind profile data were available from approximately 30 chemical releases covering sufficient altitude to employ this procedure. Data from each of these were divided into two altitude regions, $90 \lesssim z \lesssim 110$ km and $110 \lesssim z \lesssim 140$ km. A least squares fit parabola in each altitude range was subtracted from the north-south and east-west wind components to obtain the residual winds. The shear and energy spectrum functions for both total winds and residual winds were then obtained from (26) and (27). Data were also available from two releases in the 70 to 90 km altitude region, but these have not been included since the results were not statistically significant.

Figures 8 and 9 show typical shear and energy spectrum functions of the residual winds in the lower altitude range, plotted on log-log scale for easy determination of the exponent of ξ . The quantity graphed in Figure 9 is just the velocity difference part of equation (27), omitting the factor $\frac{1}{2}$. Both graphs show exponents in the small ξ region which are in reasonable agreement with the ones expected from equations (24) and (25).

The observed functions $\overline{E}_o$ and $\overline{F}_o$ of (26) and (27) are not, however,

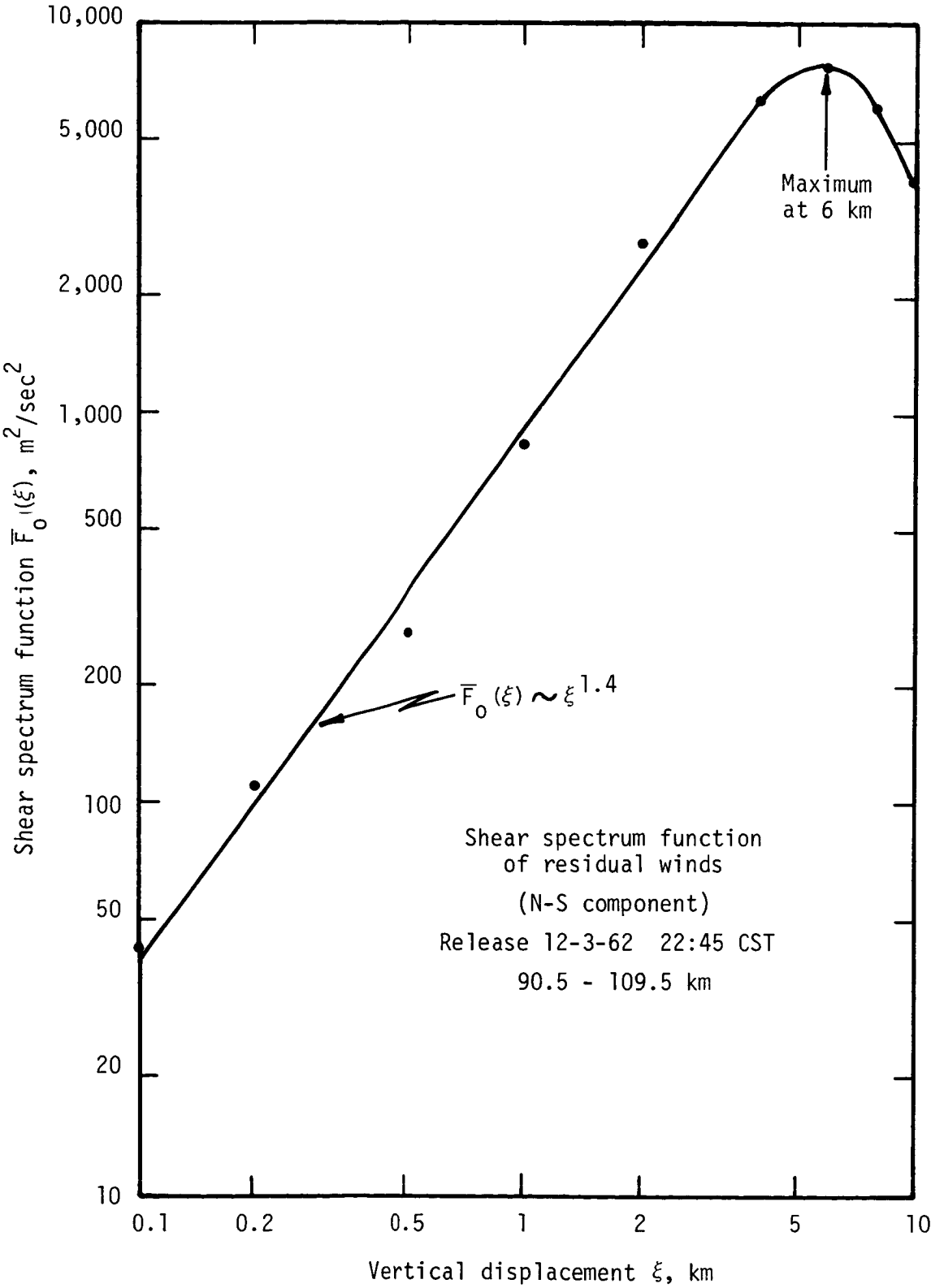

Figure 8. Sample Shear Spectrum Function of the North-South Component of the Residual Winds.

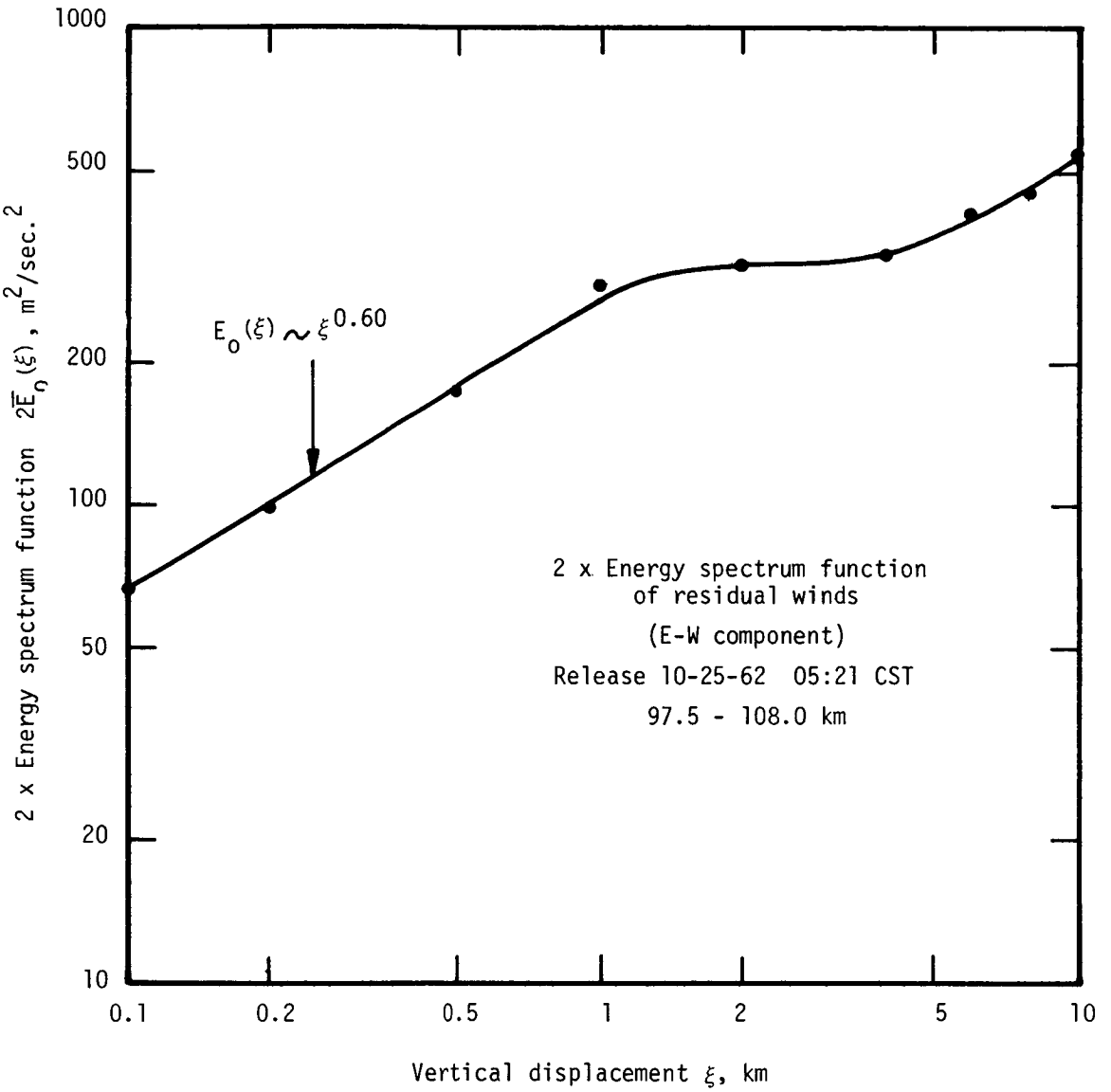

Figure 9. Sample Energy Spectrum Function (Times 2) for the East-West Component of the Residual Winds.

identical with the theoretical relations (24) and (25). Since the method of obtaining the residual winds leaves some contribution from the mean wind profile, $\overline{E}_o$ and $\overline{F}_o$ are related to $\overline{E}$ and $\overline{F}$ by

$$\overline{E}_o(k) = \varphi_1 \overline{E}(k) \tag{30}$$

and

$$\overline{F}_o(k) = \varphi_2 \overline{F}(k) \quad , \tag{31}$$

where φ_1 and φ_2 are dimensionless factors required to compensate for the contributions from the mean winds, and which increase as this contribution becomes larger.

Tables 1 and 2 show the results of averaging all of the exponents of the shear and energy spectrum functions of both total and residual winds in the two altitude regions. Averages were taken of data from all releases as well as separate averages for morning twilight and night releases.

The observed average globule cutoff altitude was 106 km for the releases studied. Thus the 90 to 110 km region embraces the turbulent zone while the 110 to 140 km range lies above the turbulent zone.

Tables 1 and 2 show that above the turbulent zone the average exponents of both shear and energy spectrum functions are higher than those expected from equations (24) and (25). In the turbulent region the exponents of both shear and energy spectrum functions are in better agreement with (24) and (25), but the values are still slightly high. The exponents obtained from the residual winds come closer to the expected values than do those of the total winds. For the total winds, the nighttime exponents of both $\overline{E}_o$ and $\overline{F}_o$ tend to be higher than the morning twilight values.

Table 1. Average Shear Spectrum Function Exponents

Height Range (km)	Total Winds			Residual Winds		
	All Releases	Twilight Releases	Night Releases	All Releases	Twilight Releases	Night Releases
≈ 90-110	1.49	1.25	1.51	1.47	1.50	1.43
≈110-140	1.74	1.75	1.74	1.55	1.59	1.51

Table 2. Average Energy Spectrum Function Exponents

Height Range (km)	Total Winds			Residual Winds		
	All Releases	Twilight Releases	Night Releases	All Releases	Twilight Releases	Night Releases
≈ 90-110	0.77	0.70	0.79	0.70	0.73	0.66
≈110-140	0.84	0.83	0.85	0.78	0.82	0.75

For the residual winds, the twilight exponents are lower than the values for nighttime, the twilight turbulent zone exponent being approximately equal to the nighttime value above the turbulent zone.

For chemical releases with many identifiable features, separate photographic tracking of these features provides several wind velocities in each kilometer section of altitude. The motion spectrum function $f(\delta)$ can be obtained by averaging velocity differences according to (28) with δ representing displacements which remain within a one kilometer altitude range of the position $\underline{r}$, of equation (28). By thus confining the averages to essentially a horizontal plane, the effects of the vertical shear can be eliminated and the non-shear turbulent motion spectrum results. This procedure has been applied to 13 chemical releases in the approximate height range 90 to 110 km. The resultant average motion spectrum function for each wind component is plotted on log-log scale in Figure 10. A superimposed line of slope 2/3 is seen to fit the data well for horizontal displacements of seven km or less. Thus equation (29) accurately describes the horizontal non-shear turbulent motion spectrum function.

The Buoyancy Subrange

According to the buoyancy theory of Bolgiano [1959], buoyancy forces act to oppose vertical motions and remove kinetic energy from the turbulence over the wave number range $k_o \leq k \leq k_B$. The predicted energy spectrum in this region is

$$E(k) = \theta \, \epsilon_g^{2/5} \, \omega_g^{4/5} \, k^{-11/5} \quad , \tag{32}$$

where θ is a dimensionless constant and ω_g was defined in Chapter I. The

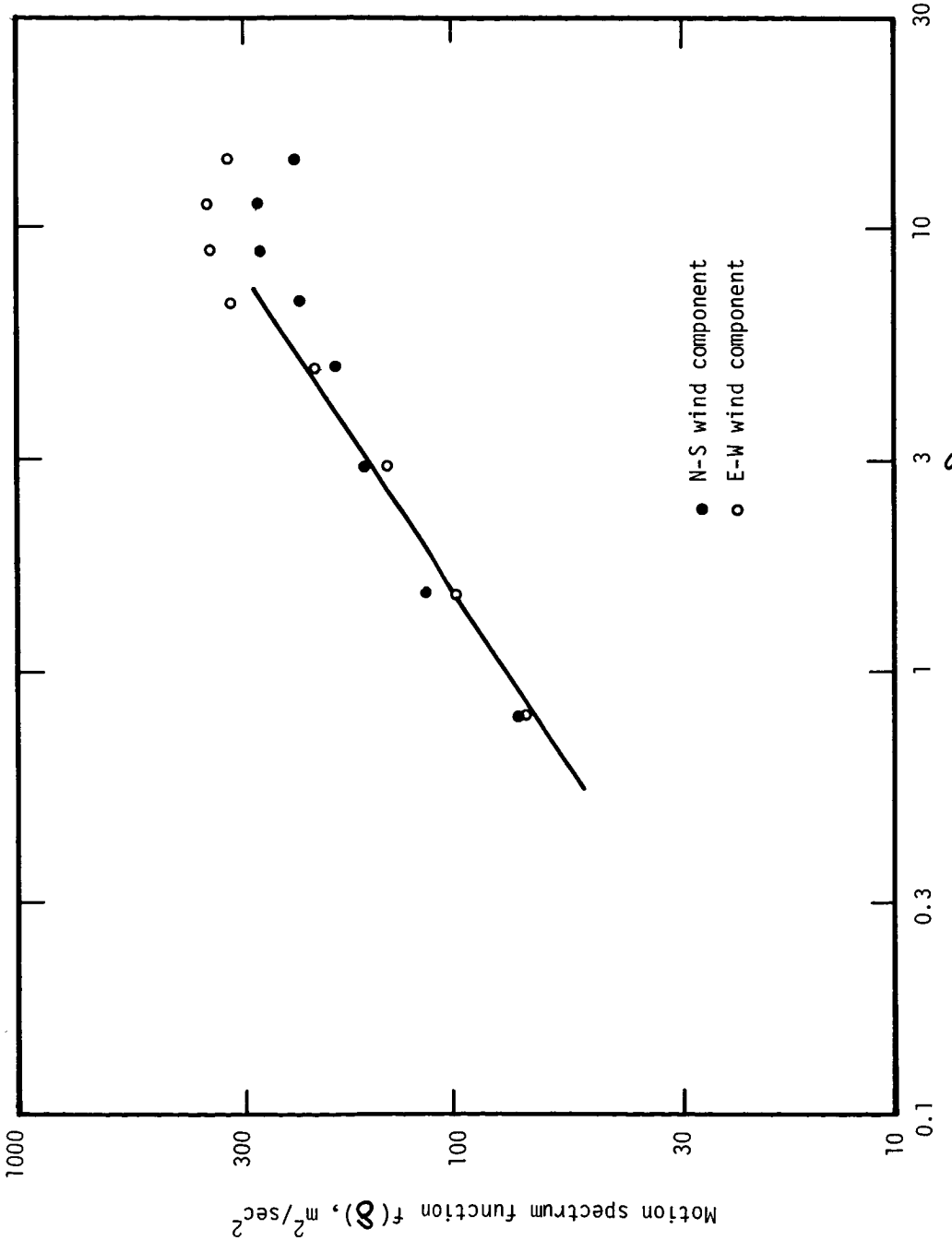

Figure 10. Average Horizontal Motion Spectrum of the Turbulent Winds.

eddy scale $L_B = k_B^{-1}$ above which the buoyancy effects become important in the Bolgiano theory is given by the relation

$$L_B = \frac{\epsilon^{5/4}}{\epsilon_g^{3/4} \omega_g^{3/2}} \quad . \tag{33}$$

If values of ϵ and ϵ_g are taken from Figure 6, and the value 2.4×10^{-2} sec^{-1} is used for ω_g, the calculated values for L_B at heights of 95, 100 and 105 km are about 1, 10 and 100 m, respectively. Since the scale of the smallest eddies $L^* = k^{*-1}$ is about 20 to 40 m in this height range, there is little or no portion of the spectrum which could form an inertial subrange in the region $k_B \leq k \leq k^*$. Therefore, the assumption that the buoyancy subrange occupies the entire wave number range $k_b \leq k \leq k^*$ is justified.

Roper [1963] has proposed a buoyancy subrange which, unlike the one predicted by Bolgiano, affects only the small scale eddies with wave numbers in the range $k_b \leq k \leq k^*$ as indicated in Figure 7(c). The largest buoyancy scale $L_b = k_b^{-1}$ is determined by requiring that in the altitude range over which buoyancy effects are important (possibly only the 90 to 110 km region), the buoyancy kinetic energy per unit mass $\frac{1}{4} L_b^2 \omega_g^2$ must be less than or approximately equal to the turbulent kinetic energy per unit mass $\frac{1}{2} v^2$. Roper's data, obtained from meteor trail wind analysis, indicate that $L_b \approx 0.7$ km. Figure 3 shows that this value is in good agreement with the observed largest buoyancy scale in the height region 98 to 106 km, as determined from globule growth studies. Since the t^5 buoyancy subrange diffusion discussed in Chapter I agrees with Bolgiano's theory, it appears that this theory adequately describes the buoyancy effects if the energy

balance large scale cutoff is included. Therefore the Bolgiano energy spectrum (32) presumably applies to the observed buoyancy subrange.

Since the energy spectrum is modified for small scales by the existence of the buoyancy subrange, the observed energy spectrum function $\overline{E}_o(\xi)$ should also be modified for $\xi \lesssim 0.7$ km. However, this effect was undoubtedly masked by the method used for obtaining $\overline{E}_o(\xi)$ for $\xi < 1$ km. These values were determined from interpolation between wind profile data points which were spaced not less than one km apart. Roper [1963] reports that spectrum analysis of turbulent winds obtained from meteor tracking does show anomalies in the scale range $\xi \lesssim 0.7$ km. The buoyancy effects may also be a contributing factor to the slightly high exponents observed for $\overline{E}_o$ and $\overline{F}_o$, since substitution of (32) into (20) would yield $\overline{E}(\xi) \sim \xi^{6/5}$ for ξ in the buoyancy subrange, a higher exponent power law than (24).

Evaluation of Constants in the Spectrum Functions

The values of the constants α and γ in the energy spectrum $E(k)$ and the motion spectrum function $f(\delta)$ may be evaluated by a refined procedure similar to one developed by Roper [1963]. The turbulence power ϵ is given by

$$\epsilon = 2\eta \int_0^\infty k^2 E(k)\, dk \quad . \tag{34}$$

Since the integral is dominated by the inertial and buoyancy subrange contributions, this is approximately

$$\epsilon = 2\eta\, \alpha\, \epsilon_s^{2/3} \int_{k_o}^{k_b} k^{1/3}\, dk + 2\eta\, \theta\, \epsilon_g^{2/5}\, \omega_g^{4/5} \int_{k_b}^{k^*} k^{-1/5}\, dk. \tag{35}$$

At k_b the inertial subrange energy spectrum (18) must equal the buoyancy subrange energy spectrum (32). This implies that

$$\theta = \frac{\alpha \epsilon_s k_b^{8/15}}{\epsilon_g^{2/5} \omega_g^{4/5}} \tag{36}$$

and that the buoyancy subrange energy spectrum (32) may be written as

$$E(k) = \alpha \epsilon_s^{2/3} k_b^{8/15} k^{-11/5} \quad . \tag{37}$$

The use of this result in (35), and the performance of the integration produces an equation which has α as the only unknown. Neglecting terms not containing k^* causes only five per cent error or less. The resultant equation, solved for α , is

$$\alpha = \frac{2 \epsilon^{4/5} L_b^{8/15}}{5 \eta^{2/5} \epsilon_s^{2/3}} \quad , \tag{38}$$

where the well known relation $k^* = (\epsilon/\eta^3)^{\frac{1}{4}}$ has been used. If values of L_b, ϵ and ϵ_s are obtained from Figures 3 and 6, and 1962 U. S. Standard Atmosphere data are used to evaluate η, equation (38) yields values of 0.6 and 1.6 for α at altitudes of 100 and 105 km, respectively.

Equation (38) can be used in (36) to produce the simpler relation for θ given by

$$\theta = \frac{2}{5}\left(\frac{\epsilon^2}{\eta \epsilon_g \omega_g^2} \right)^{2/5} \quad , \tag{39}$$

which yields values of 0.08, 0.3 and 0.8 at altitudes of 95, 100 and

105 km, respectively.

The constant γ in equation (29) for the motion spectrum function can be evaluated from Figure 10 by taking 100 km as the representative altitude, hence $\epsilon_s = 0.37\ m^2/sec^3$. The resultant value for γ is 1.5.

The turbulent motion spectrum function $f(\delta)$ may be interpreted as the horizontal equivalent of the vertical energy spectrum function $\overline{E}_o(\xi)$. Thus comparison of equations (24) and (29) shows that $\gamma = \frac{3}{2}\alpha$. Since $\gamma = 1.5$, this implies $\alpha = 1.0$, in good agreement with the average value of α determined from equation (38).

The maximum in $f(\delta)$ in Figure 10 indicates a horizontal scale of 10 km for the turbulent winds. Previously [Greenhow and Neufeld, 1959a, 1959b, 1960] the horizontal scale of the turbulent winds has been estimated as 200 km. However, Hines [1960] later attributed this horizontal scale to the gravity wave component of the total winds. The reason why this maximum in $f(\delta)$ implies a 10 km scale for the turbulent winds is discussed in the following section.

Equating the observed maximum in $f(\delta)$ ($\approx 330\ m^2/sec^2$) with $\frac{1}{2}U_o^2$, the kinetic energy per unit mass of the largest eddies, implies that $U_o = 26$ m/sec. The vertical scale at 100 km is approximately seven km, indicating only slight anisotropy of the inertial subrange due to shear influence. If the largest eddy scale L_o is taken as seven km instead of 10, evaluation of $f(\delta)$ at $\delta = 7$ km implies $U_o = 23$ m/sec. Presumably the most appropriate values for L_o and U_o are somewhere between the limits seven to 10 km and 23 to 26 m/sec.

If the value $\alpha = 1.0$ is used in equation (24), the parameter φ_1 of equation (30) can be evaluated from the observed energy spectrum function

values $\bar{E}_o$ at some displacement, say one km. The relation for φ_1 is then

$$\varphi_1 = \frac{2\,\bar{E}_o(1\text{ km})}{3(1000)^{2/3}\,\epsilon_s^{2/3}} \quad . \tag{40}$$

U_o can also be estimated by taking L_o = 7 km and requiring $\bar{E}_o(L_o) = \varphi_1(\frac{1}{2}U_o^2)$, as implied by equation (59) of Chapter III. U_o is thus given by

$$U_o = \left(\frac{2\,\bar{E}_o(7\text{ km})}{\varphi_1}\right)^{\frac{1}{2}} \quad . \tag{41}$$

Table 3 shows the resultant values for φ_1 and U_o at several altitudes. The φ_1 values are seen to decrease with increasing altitude. This would be expected since the polynomial fitting procedure used to obtain residual winds should be better for more nearly "monochromatic" upper altitude winds. The values of U_o in Table 3, although agreeing fairly well with the previous estimates, are consistently low. The U_o values in Table 3 could be reconciled with the estimate U_o = 25 m/sec by either of the not unreasonable choices α = 1.5 or ϵ_s increased by a factor of 1.8. Either of these alterations would decrease φ_1 to about two-thirds the values shown in Table 3.

The Spectrum Functions Related to Scale Size

Tchen [1954] has shown theoretically that for high shear fields both E(k) and F(k) are proportional to k^{-1}. Thus for high shear fields the relations for $\bar{E}(\xi)$ and $\bar{F}(\xi)$ would become

$$\bar{E}(\xi) \sim \ln(1/\xi) \tag{42}$$

and

Table 3. Values of φ_1 and U_o Determined from $\overline{E}_o(\xi)$

Height (km)	$2\,\overline{E}_o$(1 km) (m^2/sec^2)	$2\,\overline{E}_o$(7 km) (m^2/sec^2)	φ_1	U_o (m/sec)
90	749	1920	6.0	18
95	730	2100	5.2	20
100	698	1540	4.5	19
105	649	1420	3.8	19
110	558	1180	3.0	20

$$\overline{F}(\xi) \sim \ln(1/\xi) \tag{43}$$

instead of the low shear relations (24) and (25).

The observed shear spectrum function $\overline{F}_o(\xi)$ typically has a maximum similar to the maximum at ξ = 6 km seen in Figure 8. In the 90 to 110 km region the average ξ at maximum is seven km. Zimmerman [1962] has suggested that this maximum may represent the transition point from low shear isotropic turbulence to high shear field anisotropic shear turbulence, the shear spectrum function changing from the form in equation (25) to that given in (43). If this is the case, the $d^2 \sim t^3$ observed on globules at small scales should, according to Tchen's diffusion theory [1961], undergo a transition to $d^2 \sim t^2$ at this scale size, in agreement with Cote's [1965] observations. However, Blamont and de Jager [1961] proposed that the maximum in $\overline{F}_o$ corresponds to the vertical correlation distance of the motion field.

It is instructive to consider a hypothetical velocity profile $v(\zeta) = C \sin(\zeta)$, where C is a constant amplitude and ζ is an appropriate nondimensional altitude. For this case, the shear spectrum function would be

$$\overline{F}_o(\delta\zeta) = \frac{C^2}{2\pi} \int_0^{2\pi} [\sin(\zeta) - \sin(\zeta + \delta\zeta)]^2 \, d\zeta$$

$$= C^2 [1 - \cos(\delta\zeta)] \quad . \tag{44}$$

If this relation is plotted on log-log scale, the resultant curve is qualitatively similar to the curve for $\overline{F}_o$ in Figure 8. A maximum occurs at $\delta\zeta = \pi$ (that is, at one half the wave length), but the $\overline{F}_o$ of (44) is proportional to $(\delta\zeta)^{2.0}$ in the small $\delta\zeta$ region.

The actual wind profiles (either total or residual) contain components of more than one wave length, but it seems reasonable to assume that the shear spectrum function maximum should still be associated with the scale of the predominant wave length (or wave lengths) of the components. This conclusion is supported by the fact that a similar maximum at δ = 10 km occurs in the horizontal motion spectrum function $f(\delta)$ in Figure 10. This indicates a horizontal scale for the turbulence of about 10 km although there is no high shear field which can be associated with the horizontal displacements. The shear and motion spectrum scales will be discussed more thoroughly in the next chapter. The fact that the $\overline{E}_o(\xi)$ curves do not generally have a well defined maximum like that of the $\overline{F}_o(\xi)$ curves, and hence show no transition from relation (24) to (42), also supports the conclusion that the $\overline{F}_o(\xi)$ and $f(\delta)$ maximums are to be associated with a length scale of the motion.

CHAPTER III

CHARACTERISTIC SCALES OF THE MOTION

Definitions of the Length Scales

The characteristic time and length scales of the turbulent eddies are important parameters of the turbulent velocity field. The chemical release method provides two means of determining these scales: (1) direct observation of the globules or structure of the chemical clouds in the turbulence and (2) determination of the scales by analysis of the wind velocities and fluctuations.

Two important characteristic length scales are L_o, the scale of the largest, energy bearing eddies (wave number k_o) and L^*, the scale of the smallest, energy dissipating eddies (wave number k^*).

Vertical Autocorrelation Scale

The vertical autocorrelation coefficient $G(\delta z)$ for the total wind profile $V(z)$ is defined as

$$G(\delta z) = \frac{\langle V(z)\, V(z+\delta z)\rangle}{\left\{\langle [V(z)]^2\rangle \langle [V(z+\delta z)]^2\rangle\right\}^{\frac{1}{2}}} , \qquad (45)$$

where averages are taken over a range of altitudes z. Relation (45) is appropriate for wind profiles $V(z)$ for which the average over altitude $\bar{V}$ is zero. If $\bar{V}$ is not zero than $V(z) - \bar{V}$ must be substituted for $V(z)$ throughout this formula. To see how G. is related to a length scale of the motion, consider a hypothetical wind profile given by $V(\zeta) = C \sin(\zeta)$,

where C is a constant amplitude and ζ is an appropriate nondimensional altitude. For this "monochromatic" profile $G(\delta\zeta)$ would be

$$G(\delta\zeta) = \frac{C^2\int_0^{2\pi} \sin(\zeta)\,\sin(\zeta + \delta\zeta)\,d\zeta}{C^2\int_0^{2\pi} \sin^2(\zeta)\,d\zeta} = \cos(\delta\zeta) \quad . \tag{46}$$

Thus $G = 1$ at $\delta\zeta = 0$ and $G = 0$ at $\delta\zeta = \pi/2$, that is at one quarter wave length. An actual wind profile is made up from components of many wave lengths but a general cosine-like dependence is still observed for $G(\delta z)$. The value of δz at which $G(\delta z)$ first attains the value zero is called the vertical autocorrelation scale, L_v.

Shear and Motion Spectrum Scales

The observed shear spectrum function $\overline{F}_o(\xi)$ and the motion spectrum function $f(\delta)$ were defined in Chapter II, where ξ is a vertical displacement and δ is a horizontal displacement. The shear and motion spectrum scales, L_S and L_s, are defined as the values of ξ and δ at which $\overline{F}_o(\xi)$ and $f(\delta)$ attain a maximum value. It was shown in Chapter II that for a "monochromatic" velocity profile this maximum would occur at ξ or δ equal to one half the wave length. Thus, for a "monochromatic" velocity profile, the vertical shear spectrum scale should be twice the vertical autocorrelation scale.

Mixing Length Scale

An analogy between random molecular and turbulent motions introduces the concept of mixing length. According to the mixing length idea of turbulent motion, eddies in fully developed turbulence transport momentum from

one level of the flow to another. The transport of momentum from the level z to the level $z + L_m$ produces a velocity fluctuation v in the mean velocity V according to the relation

$$v = V(z + L_m) - V(z) \approx L_m \frac{\partial V}{\partial z} , \tag{47}$$

where L_m is the mixing length. Thus the magnitude of the mixing length is given approximately by

$$L_m = \frac{v}{\left(\frac{\partial V}{\partial z}\right)} , \tag{48}$$

where v is the magnitude of the observed turbulent velocity.

Viscous Cutoff Scales

Standard theories of homogeneous turbulence provide a method of evaluating the length and time scales of the smallest eddies, those which dissipate their kinetic energy by viscous action. The length scale of these eddies is given by

$$L^* = \left(\frac{\eta^3}{\epsilon}\right)^{\frac{1}{4}} , \tag{49}$$

and the time scale by

$$\tau^* = \left(\frac{\eta}{\epsilon}\right)^{\frac{1}{2}} , \tag{50}$$

where η is the kinematic viscosity of the atmosphere and ϵ is the rate per unit mass at which energy is dissipated by viscous forces.

Spatial Correlation Scales

The one dimensional correlation coefficient of the turbulent winds is defined by

$$g(\xi) = \frac{\langle v(\underline{x})\ v(\underline{x} + \underline{\xi})\rangle}{\left\{\langle [v(\underline{x})]^2\rangle\langle [v(\underline{x} + \underline{\xi})]^2\rangle\right\}^{\frac{1}{2}}} \tag{51}$$

where the averages are taken over positions $\underline{x}$, and $\underline{\xi}$ is a spatial displacement. There are actually two pertinent one dimensional correlation coefficients $g_1(\xi)$ and $g_2(\xi)$, the longitudinal and transverse correlations, where $\underline{\xi}$ is respectively parallel and perpendicular to the component v which is being correlated. The scale of the largest, energy bearing eddies is given by the integral scale of these correlation coefficients. The defining equations are

$$L_o = 2\int_0^\infty g_1(\xi)\, d\xi \tag{52}$$

and

$$L_o = \int_0^\infty g_2(\xi)\, d\xi \quad . \tag{53}$$

From standard homogeneous turbulence theory [see Nawrocki and Papa, 1963] it can be shown that, to second order, g_1 and g_2 are given by

$$g_1(\xi) = 1 - \frac{\xi^2}{2\, L_d^2} \tag{54}$$

and

$$g_2(\xi) = 1 - \frac{\xi^2}{L_d^2} \quad , \tag{55}$$

where L_d is the dissipation length parameter defined by

$$L_d^2 = \frac{2\langle v_x^2 \rangle}{\left\langle \left(\frac{\partial v_x}{\partial y}\right)^2 \right\rangle} = \frac{\langle v_x^2 \rangle}{\left\langle \left(\frac{\partial v_x}{\partial x}\right)^2 \right\rangle} \quad . \tag{56}$$

L_d is a scale larger than L^* and smaller than L_o. It corresponds to eddies which contain a negligible portion of the total energy and are responsible for a negligible part of the total dissipation of energy. Solving for $\left(\frac{\partial v_x}{\partial y}\right)^2$ from equation 10 of Chapter I, and using $U_o^2 = 3\langle v_x^2 \rangle$ allows equation (56) to be written as

$$L_d^2 = \frac{5\,\eta\,U_o^2}{\epsilon} \quad . \tag{57}$$

Frequently the symbol U_o is used for the rms velocity $\sqrt{\langle v_x^2 \rangle}$. In this notation equation (57) would have a numerical factor of 15 instead of 5. Here, however, U_o refers to the total turbulent velocity and not merely the x component. For isotropic turbulence $\langle v_x^2 \rangle = \langle v_y^2 \rangle = \langle v_z^2 \rangle$. Hence, the approximate relation $U_o^2 = 3\langle v_x^2 \rangle$ may be used to obtain (57) in the present notation.

Since the total turbulent kinetic energy per unit mass ρ_E is proportional to U_o^2, and since the rate $\frac{d\rho_E}{dt}$ at which this kinetic energy is converted to internal energy by viscous forces is proportional to ϵ , then equation (57) requires the fractional rate of energy dissipation $\frac{1}{\rho_E}\frac{d\rho_E}{dt}$ to satisfy the relation

$$\frac{1}{\rho_E}\frac{d\rho_E}{dt} \sim \frac{\eta}{L_d^2} \quad . \tag{58}$$

Relation (58) justifies the name dissipation length parameter for L_d.

Relationships Among the Eddy Scales

The three eddy scales L^*, L_d and L_o are not entirely independent of one another, and relationships among these scales can be derived. By integrating the energy spectrum $E(k)$ one can obtain the kinetic energy per unit mass of the energy bearing eddies, that is

$$\tfrac{1}{2}U_o^2 = \int_0^\infty E(k)\, dk \approx \bar{E}(L_o) \quad . \tag{59}$$

Use of the form for $E(k)$ given by (18) and (32) and evaluation of the integral in (59) shows that to a good approximation the terms in k^* and k_b can be neglected. This leads to the approximate result

$$\tfrac{1}{2}U_o^2 = \tfrac{3}{2}\alpha\, \epsilon_s^{2/3}\, k_o^{-2/3} \quad . \tag{60}$$

Substituting L_o for k_o^{-1} and solving for ϵ_s yields the relation

$$\epsilon_s = (3\alpha)^{-3/2}\frac{U_o^3}{L_o} \quad . \tag{61}$$

One of the formulas of standard turbulence theory is

$$\epsilon_s = A\,\frac{U_o^3}{L_o} \quad , \tag{62}$$

where A is a dimensionless constant of order unity. If the value $\alpha = 1$

is used as an average of those obtained in Chapter II, relation (61) implies that $A \approx 0.2$.

If the relation for L_d^2 given by (57) is combined with (61), this produces the equation relating L_d and L_o, given by

$$\frac{L_d^2}{L_o} = 5\,(3\,\alpha)^{3/2}\left(\frac{\eta}{U_o}\right)\left(\frac{\epsilon_s}{\epsilon}\right) \quad . \tag{63}$$

If ϵ, obtained from equation (57), is also substituted into (49), this produces the relationship between L^* and L_d given by

$$\frac{L^{*2}}{L_d} = \frac{\eta}{\sqrt{5}\,U_o} \quad . \tag{64}$$

Equations (63) and (64) may be combined to produce a relationship among all three length scales, as given by

$$L^{*2} = \left(\frac{\epsilon}{\epsilon_s}\right)\frac{L_d^3}{(15\,\alpha)^{3/2}\,L_o} \quad . \tag{65}$$

This corresponds to the relation

$$L^{*2} = \frac{L_d^3}{10\sqrt{15}\,L_o} \tag{66}$$

derived by Townsend [1956] for isotropic homogeneous turbulence with no buoyancy subrange.

The Buoyancy Subrange Scale

Roper [1963] has predicted a buoyancy subrange which becomes most important when the buoyancy kinetic energy per unit mass is of the same magnitude as the turbulent kinetic energy per unit mass. The buoyancy kinetic energy per unit mass is, as derived in Appendix B,

$$\tfrac{1}{2} v_b^2 = \tfrac{1}{4} L_b^2 \omega_g^2 \quad , \tag{67}$$

where L_b is the characteristic largest scale of the buoyancy subrange, and ω_g, as defined in Chapter I, is the frequency at which a fluid element would oscillate when displaced from its equilibrium altitude. Since $\frac{1}{2} v_b^2$ must be less than, or at most approximately equal to the observed turbulent kinetic energy per unit mass $\frac{1}{2} v^2$, it follows that

$$L_b \lesssim \frac{\sqrt{2}\, v}{\omega_g} \quad , \tag{68}$$

where v is the average observed turbulent velocity. The eddies of size less than L_b are affected by the Roper buoyancy subrange. Over the height range from 100 to 110 km ω_g is approximately 2.5×10^{-2} sec^{-1}. Thus, use of the observed value v = 15 m/sec in relation (69) yields a value of about 0.8 km for L_b. This value is in good agreement with the observed L_b values in Figure 3 for the altitude region from 98 km to the turbopause at 106 km.

Time Scales

The time correlation coefficient of the turbulent wind component v is defined as

$$g(\delta t) = \frac{\langle v(t)\, v(t+\delta t)\rangle}{\left\{\langle [v(t)]^2\rangle \langle [v(t+\delta t)]^2\rangle\right\}^{\frac{1}{2}}} \quad , \tag{69}$$

and the time scale τ of the turbulent winds is the first value $\delta t = \tau$ at which $g(\tau) = 0$. If an eddy of size scale L_e has a characteristic velocity v_e, then its time scale τ_e is given approximately by

$$L_e = v_e \tau_e \quad . \tag{70}$$

Experimental Observations

The total winds are composed of prevailing, 24 hour and shorter period tidal components, gravity wave and turbulent components. Greenhow and Neufeld [1959a, 1959b, 1960] report large scale anisotropic turbulence with vertical scale ≈ 6 km, horizontal scale ≈ 200 km and time scale ≈ 100 min. There is some doubt (see Appendix A) as to whether the motions of this scale contain true turbulent components. Gravity wave theory [Hines, 1960] apparently accounts for these observed scales satisfactorily. The conclusion of Chapter II that near 100 km the vertical and horizontal scales of the turbulence are about 7 and 10 km supports the gravity wave explanation for the 200 km horizontal scale observed by Greenhow and Neufeld.

The vertical scale of the total winds and large scale non-tidal components may be calculated by using the total and residual winds in the vertical autocorrelation formula (45). The wind data were divided into overlapping altitude segments of 20 km and the vertical scale was calculated at five km intervals. Figure 11 shows the average results obtained from 18 chemical release profiles. The solid curve shows the vertical

autocorrelation scale of the total winds in the altitude range from 80 to 160 km. Total wind scales above 140 km were estimated by extrapolation of the vertical autocorrelation curves to their zero point and may be somewhat in error. Two values of vertical scales obtained by Webb [1964] at lower altitudes indicate continuity of the vertical scale of the total winds between lower and upper altitudes with an exponential increase in the lower region. From 80 to 140 km the vertical autocorrelation scale of the total winds is seen to follow closely the variation of the pressure scale height, as suggested by Zimmerman [1964]. The calculated vertical autocorrelation scale of the residual winds is also shown in Figure 11.

Figure 12 shows the calculated shear spectrum scale for both total and residual winds for altitudes up to 150 km. The shear spectrum scale of the total winds is also seen to follow the variation of the scale height in the region 80 to 125 km. Table 4 shows the observed ratio between the shear spectrum scale and the vertical autocorrelation scale. Below 100 km this ratio is close to unity. Above 100 km this ratio is approximately two, as expected for a "monochromatic" wind profile.

The facts that the winds below the turbopause are distinctly multiple wave length forms and that the observed spectrum functions $\overline{E}_o(\xi)$ and $\overline{F}_o(\xi)$ agree with turbulence theory predictions mean that in this height region the vertical scale of the residual winds is virtually identical to the vertical scale of the turbulence.

The turbulent winds may be obtained by individual tracking of globules or other identifiable features on the chemical release clouds. Using these turbulent velocities and vertical shears obtained from total wind profiles, one may use equation (48) to calculate the mixing length.

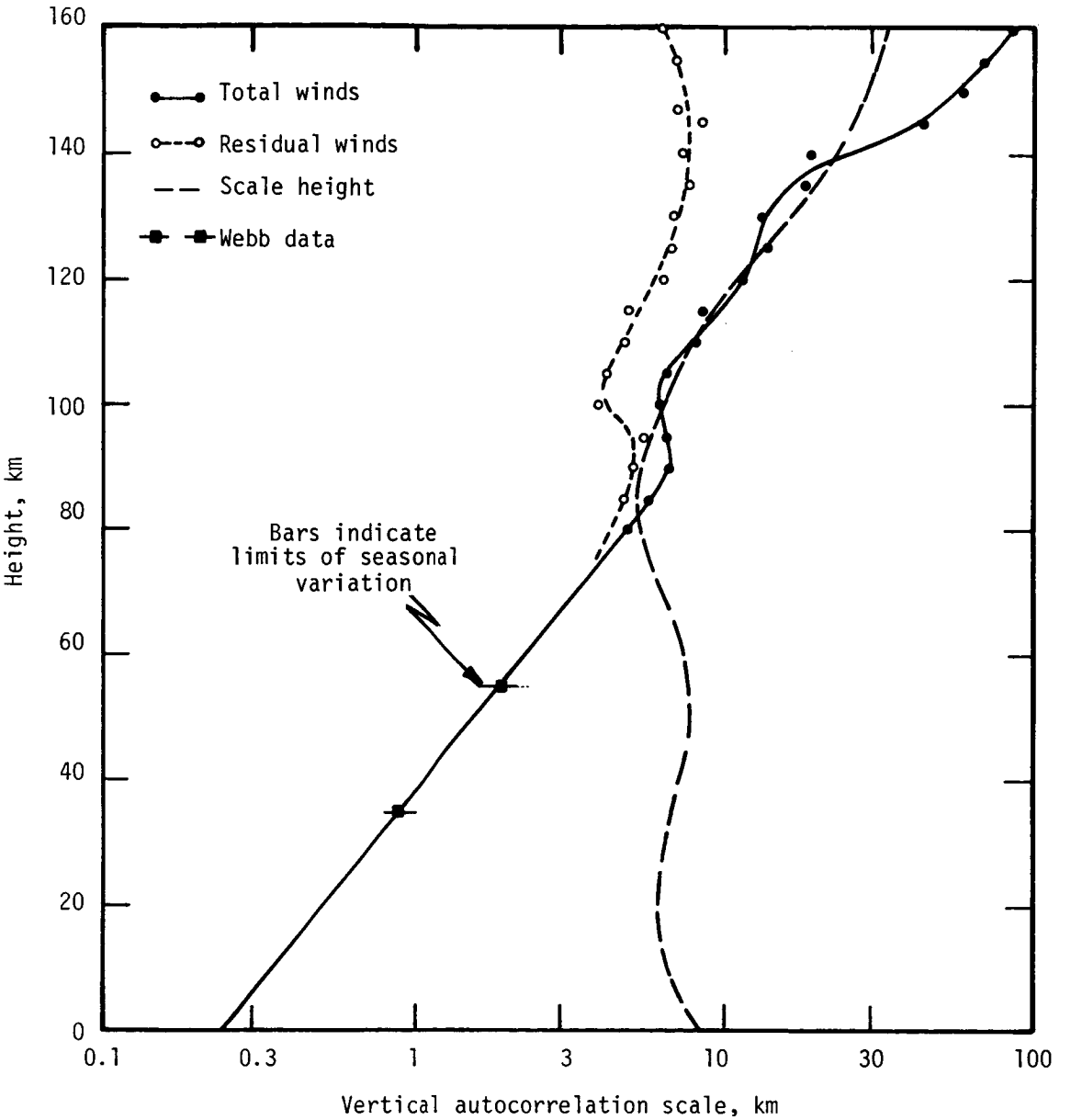

Figure 11. Vertical Autocorrelation Scale of the Total and Residual Winds.

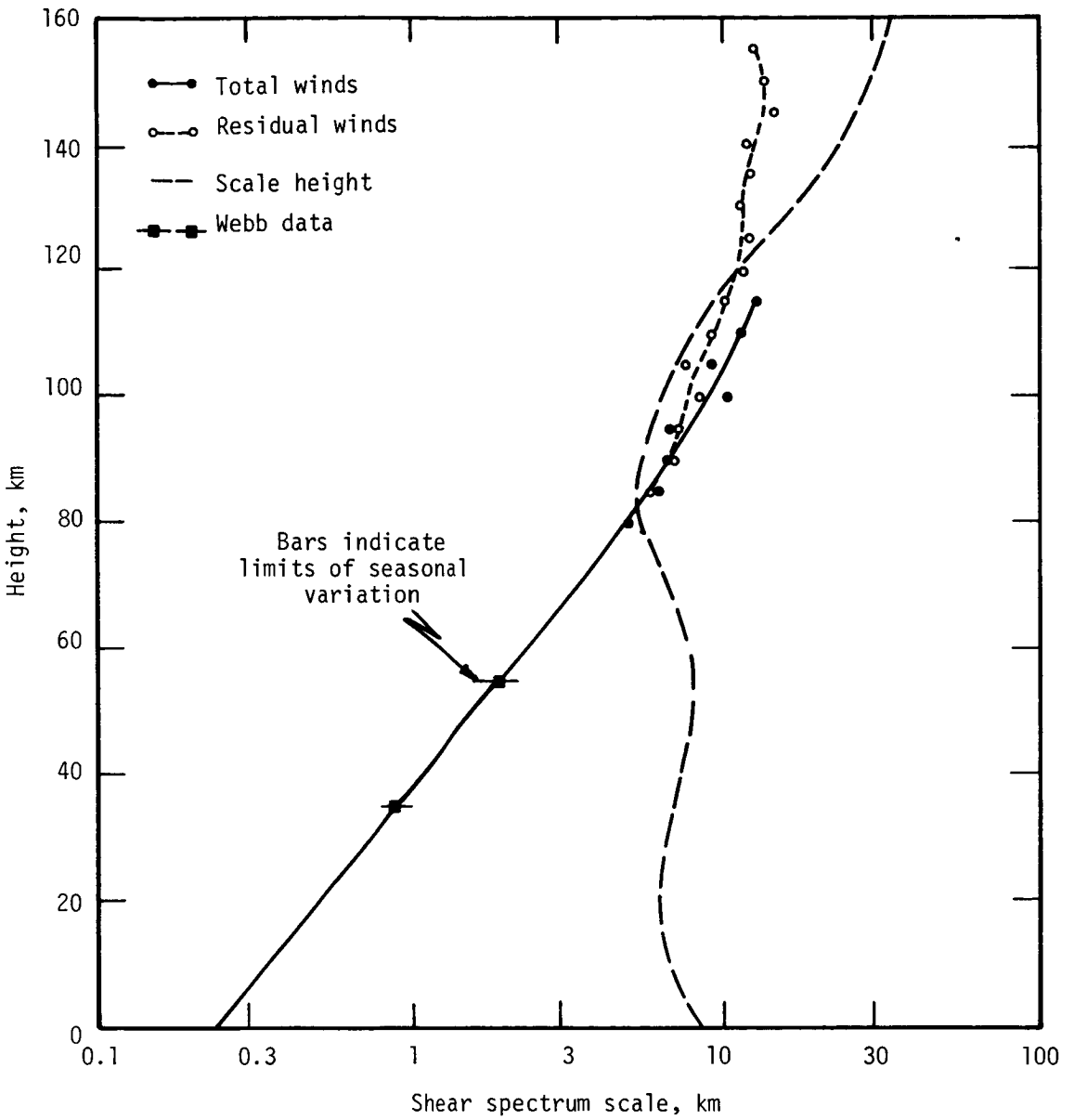

Figure 12. Vertical Shear Spectrum Scale of the Total and Residual Winds.

Table 4. Ratio of Shear Spectrum Scale to Vertical Autocorrelation Scale for Total and Residual Winds

Height (km)	Total Winds	Residual Winds
80	1.00	-
85	1.07	1.23
90	0.98	1.35
95	1.02	1.27
100	1.68	2.15
105	1.36	1.77
110	1.41	1.96
115	1.49	2.02
120	-	1.84
125	-	1.77
130	-	1.64
135	-	1.56
140	-	1.60
145	-	1.71
150	-	1.86
155	-	1.75

Figure 13 shows the calculated mixing length in the height region from 92 to 111 km. It is seen from Figure 13 that the mixing length oscillates about a constant value of approximately 0.75 km up to the turbopause region and then increases rapidly above that altitude. Thus the mixing length and the largest buoyancy subrange scale L_b are about equal in the height region immediately below the turbopause.

The viscous cutoff scales can be estimated from equations (49) and (50) by using data for ϵ obtained from Figure 6. Table 5 lists some values for L^* and τ^* calculated in this manner and v^*, the characteristic velocity of the smallest eddies, as determined by equation (70). Size and time scales, as well as velocity fluctuations of this magnitude are not observable with present techniques of chemical release observation. The smallest globules observed on the chemical releases studied for this report were about 200 m in diameter. Smaller globules could not be resolved with the short (7 inch) focal length cameras used. However, Blamont and de Jager [1961] have reported observations of globules as small as 90 m in diameter using higher resolution photography.

Use of the time varying winds over the lifetime of the chemical release to obtain turbulent velocities limits the observations to the middle portion of the turbulent spectrum. The smallest scale wind motions are excluded because of the finite time intervals (usually 15 or 30 seconds) between successive cloud position determinations. Any very large scale turbulent velocity fluctuations which may exist would be excluded because of the short usable lifetime of the chemical clouds (usually not more than about 10 min). However, it appears that most, if not all, of the larger scale turbulent fluctuations can be observed in this time period. For a

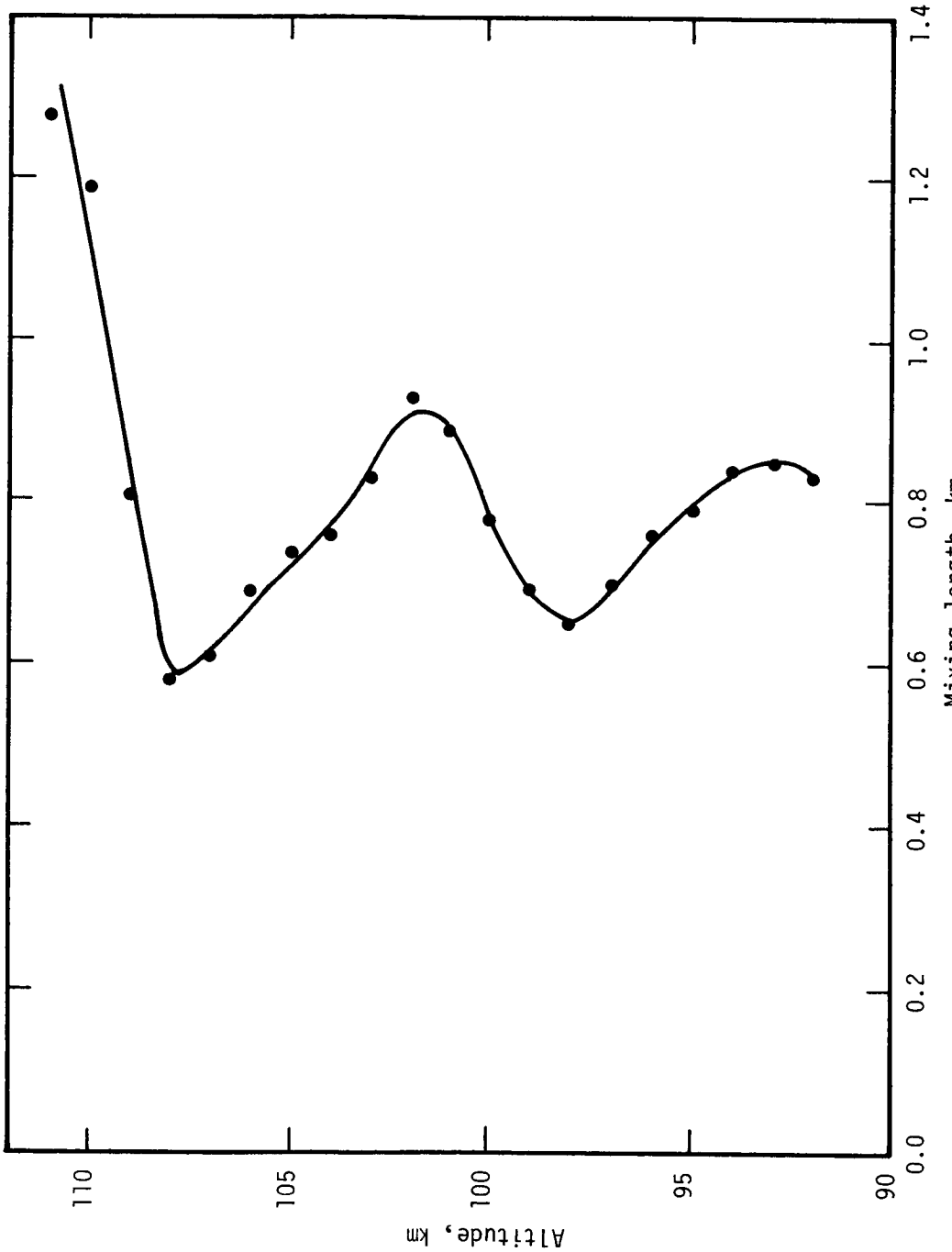

Figure 13. Mixing Length Scale versus Altitude.

largest turbulence scale L_o = 7 to 10 km with characteristic velocity 23 to 26 m/sec, as indicated in Chapter II, the time scale of the largest eddies would be 300 to 400 sec. In this case cloud observations over 10 minutes or longer would allow ample time for measurements of the largest eddies.

Figures 14 and 15 show two presentations of the observed turbulent velocity spectrum. Figure 14 shows the fraction of the observed turbulent velocities with magnitudes between one m/sec limits versus velocity from 0 to 50 m/sec. Figure 15 shows the fraction of observed turbulent velocities greater than a given velocity v, versus v from 0 to 50 m/sec. The appearance of the graph in Figure 14 below the maximum at a velocity of about eight m/sec is affected by the loss of small scale resolution and by velocity errors in the technique used for measuring the turbulent winds.

The turbulent velocities can be used in (51) to calculate the spatial correlation function. An approximation to the longitudinal correlation coefficient g_1 can be made by considering north-south velocity correlations between points separated by less than two km in both east-west and vertical directions, and similarly for east-west wind components using points separated by less than two km in both north-south and vertical directions. Figure 16 shows the average results for $g_1(ns)$ and $g_1(ew)$ versus the horizontal separation distance r. The correlation curves of Figure 16 do not have the standard form for a longitudinal correlation coefficient in isotropic turbulence. There is a similarity, however, with the form given by Townsend [1956] for isotropic turbulence consisting of eddies of only two distinct sizes. The rapid decorrelation in the region $r < 2$ km shown in Figure 16 may be a result of the buoyancy subrange influence at

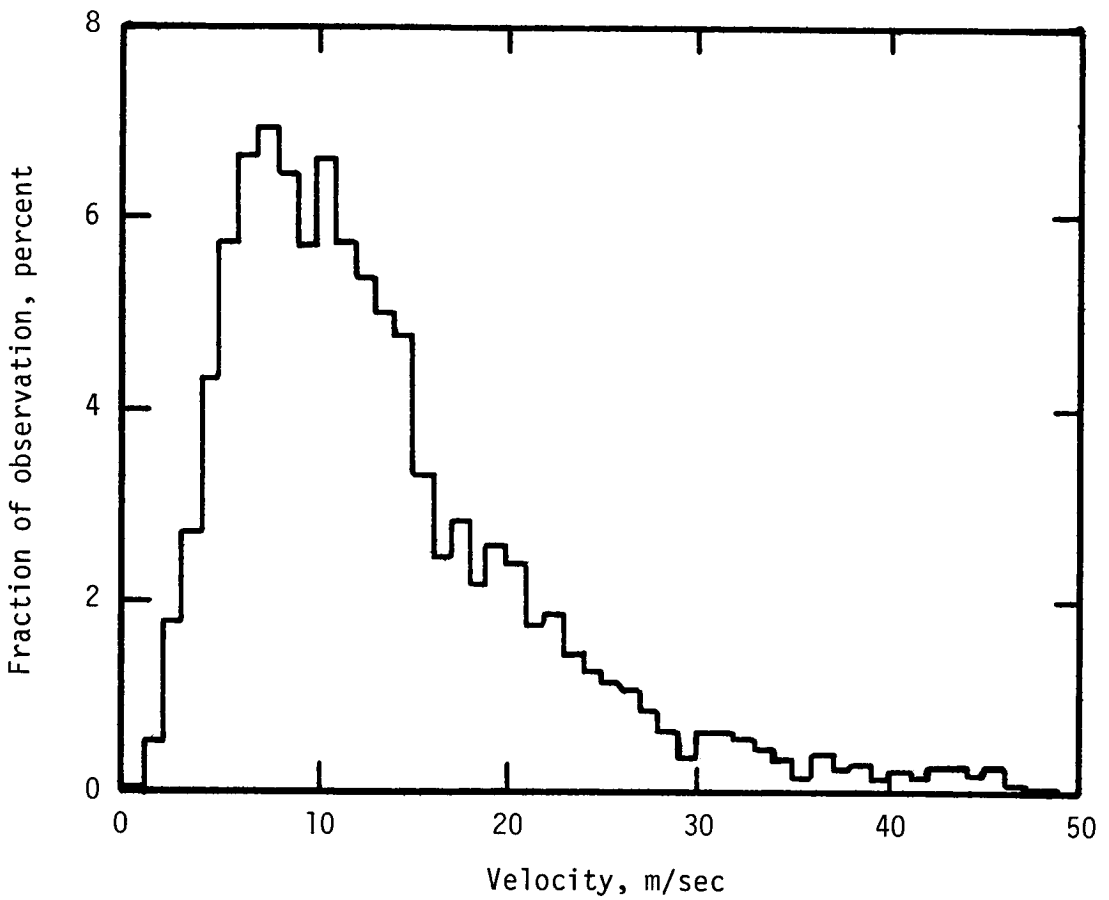

Figure 14. The Fraction of Observed Turbulent Velocities in one m/sec Intervals versus Velocity.

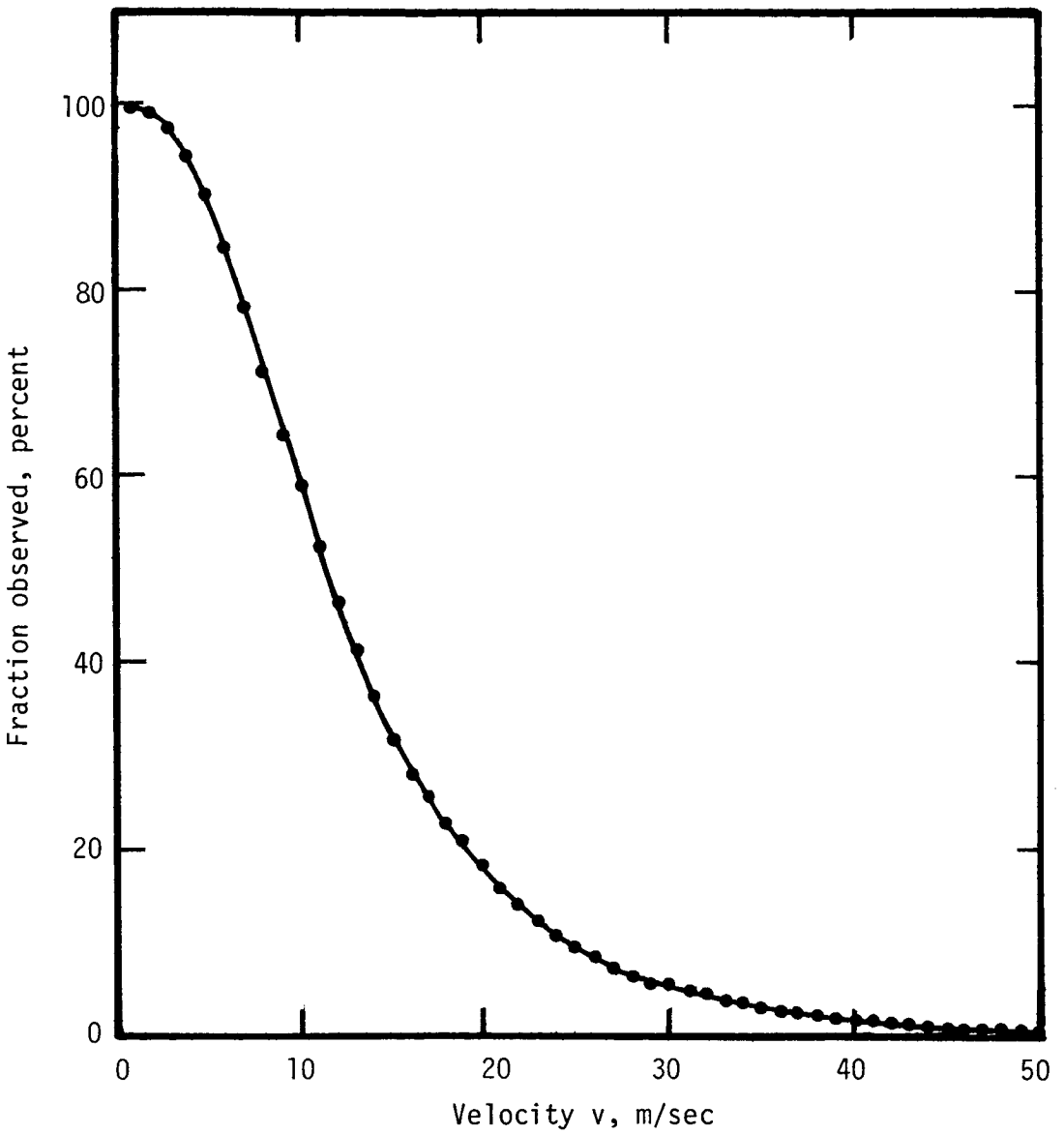

Figure 15. The Fraction of Observed Turbulent Velocities Greater than a Given Value v, versus v.

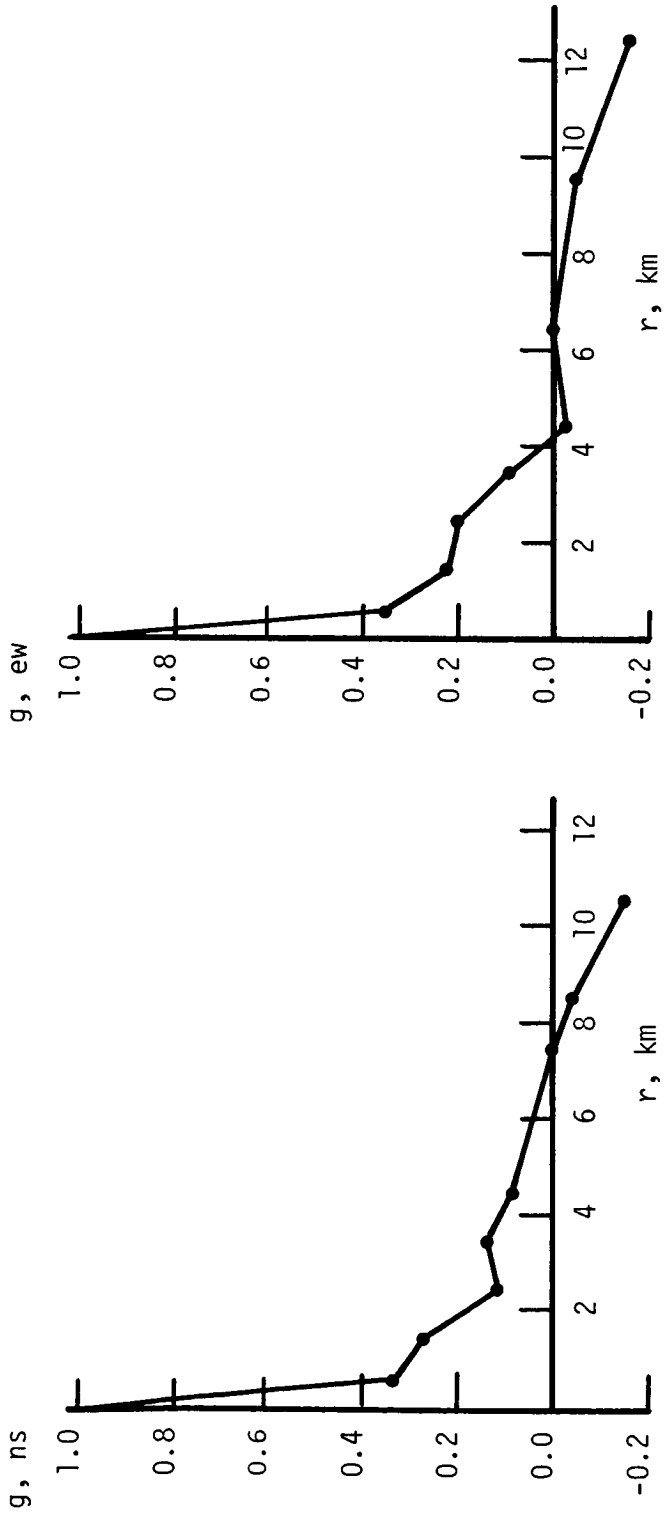

Figure 16. Spatial Correlation Function for North-South and East-West Turbulent Wind Components versus Horizontal Spatial Displacement.

small scales or, more probably, the result of limited accuracy in determining the turbulent velocities. The rms observed turbulent velocity is about 15 m/sec and the average error in turbulent wind determinations is about five m/sec. Because of these uncertain anomalies, the correlation curves of Figure 16 cannot be used to obtain reliable estimates of the integral scale L_o or the dissipation length parameter L_d. However, the fact that the zero points on the curves of Figure 16 are at about six km does verify that L_o must be of this order of magnitude for horizontal displacements.

Since wind shears tend to stretch the chemical clouds into more or less horizontal configurations, it is easier to find points for correlation with horizontal rather than vertical separations. However, the vertical spatial correlation has been calculated in a similar fashion to the horizontal correlation by considering vertical velocity component correlation only between points separated by less than two km in both horizontal directions. Because of the few correlation points obtainable, the vertical spatial correlation curve has a more ragged appearance than the graphs of Figure 16 and hence is not shown here. However, it has quite similar features of rapid decorrelation at the small displacements and a zero point at less than six km.

By using U_o = 25 m/sec and data from Chapter I for η and ϵ, one can employ equation (57) to obtain the values of L_d shown in Table 5. If α = 1 and ϵ_s = 0.37 m^2/sec^3 are chosen as appropriate values, equation (61) yields the value 8.2 km for L_o, in good agreement with the estimates made in Chapter II. Relating U_o and L_o by equation (70) implies that the time scale τ_o of the largest eddies is about 330 sec. Direct time corre-

lation of the turbulent velocities by relation (69) shows a correlation scale of about 300 sec, in good agreement with this value for τ_o.

As discussed in Chapter I, the time required for globules to diffuse to their leveling off diameter, which corresponds to L_b, is 150 $\pm$ 40 sec. The globules remain in the level phase for about 50 sec, that is, until 200 $\pm$ 40 sec after the release of the chemical cloud. The period of harmonic oscillation for a fluid element displaced from its equilibrium altitude is $2\pi/\omega_g$, which ranges in value from 250 to 285 sec in the altitude from 85 to 110 km. Thus the globules remain under the influence of the buoyancy subrange for an appreciable fraction of an oscillation period.

Layzer [1961] has argued that if a fluid element retains its identity for a length of time equal to a major part of a complete oscillation period, then the motion is not true turbulence. The harmonic oscillations caused by the buoyancy subrange are certainly too ordered to be considered random turbulent motions. However, Layzer's argument is based on the Bolgiano buoyancy theory which allows the buoyancy subrange to affect large scales of the motion and possibly to produce motions which are larger in magnitude than the random turbulent fluctuations. Since the observed buoyancy subrange is confined to the small scale range, its regular velocities are always smaller in magnitude than the random fluctuations and the total irregular velocity fluctuations retain the randomness necessary for turbulent motions.

Taking equation (67) as the definition of the characteristic velocity v_b of the largest buoyancy scale L_b, and using (70) to calculate τ_b, one can obtain the result

$$\tau_b = \frac{\sqrt{2}}{\omega_g} \quad . \tag{71}$$

In the region near 100 km (71) yields a value of about 57 sec, in good agreement with the observed time which the globules spend in the level phase.

Table 5. Summary of Altitude Dependent Viscous Cutoff Length and Time Scales, and the Dissipation Length L_d

Height (km)	L^* (m)	τ^* (sec)	v^* (m/sec)	L_d (km)
92	17	51	0.3	2.9
94	19	44	0.5	2.4
96	22	37	0.6	2.1
98	24	31	0.8	1.7
100	26	25	1.0	1.4
102	30	23	1.4	1.3
104	33	18	1.8	1.0
106	35	14	2.1	0.8

CHAPTER IV

CRITERIA FOR THE ONSET OF TURBULENCE

In Chapter I the turbulence cutoff altitude, the turbopause, near 106 km was justified by energy balance considerations. The turbopause can also be justified, though not as rigorously, by stability considerations. In a region of the atmosphere where the temperature is stably stratified, such as above the mesopause at about 85 km, the temperature structure cannot provide the instability or energy necessary for maintaining turbulence. This instability and energy can be provided only by wind shears. In such cases the Richardson criterion and possibly the Reynolds criterion for the onset of turbulence must be satisfied in order for turbulence to be present.

The Reynolds Criterion

In a fluid characterized by length scale L, density ρ , characteristic velocity v and kinematic viscosity η the inertia force per unit volume is

$$F_i = \frac{C_i \rho v^2}{L} \tag{72}$$

and the friction or viscous force per unit volume is

$$F_f = \frac{C_f \eta \rho v}{L^2} \quad , \tag{73}$$

where C_i and C_f are dimensionless constants. Blamont and de Jager [1961]

have proposed that a necessary but not sufficient condition for the existence of turbulence in a free atmosphere is that the Reynolds number defined by

$$Re = \frac{C_f F_i}{C_i F_f} = \frac{v L}{\eta} \tag{74}$$

be greater than some critical value Re_{crit}. Flow experiments in cylindrical tubes show $Re_{crit} \approx 2000$ if L is taken to be the tube diameter and v the average flow velocity. However, Hines [1963] has raised some theoretical questions as to the validity of the Reynolds criterion for free atmosphere flow. In addition to these problems, the relevant values of L and v to be used in the free atmosphere Reynolds number are not known. Also the correct critical value for a free atmosphere is uncertain. Thus the criterion $Re > Re_{crit}$, even if appropriate, cannot be used as a rigorous necessary condition for the existence of turbulence. Nonetheless, if the Reynolds criterion is accepted as necessary, it can be used to give at least a plausibility argument for the validity of the 106 km observed turbopause.

One possible choice of velocity and length scales is U_o and L_d, the characteristic velocity of the largest eddies and the dissipation length, discussed in Chapter III. This choice defines the turbulence Reynolds number

$$Re_t = \frac{U_o L_d}{\eta} \quad . \tag{75}$$

Blamont and de Jager [1961] made the choice $\bar{V}$, the average total wind speed, and L_H, the pressure scale height, shown in Chapter III to be

equivalent to the vertical autocorrelation scale. This choice yields the total winds Reynolds number

$$Re_T = \frac{\bar{V} L_H}{\eta} \quad . \tag{76}$$

Two possible "hybrid" Reynolds numbers which can be formed by alternate combinations of these characteristic length and velocity values are

$$Re_o = \frac{U_o L_H}{\eta} \tag{77}$$

and

$$Re_d = \frac{\bar{V} L_d}{\eta} \quad . \tag{78}$$

U_o was shown to be about 25 m/sec in Chapters II and III. Values of L_H and L_d were also given in Chapter III. $\bar{V}$ can be evaluated by averaging over the wind speeds obtained at a given altitude from several chemical releases. Figure 17 shows the calculated height variation of the four Reynolds numbers of equations (75) through (78). An assumed value of 2000 for Re_{crit} is shown as a vertical dashed line in the figure. This value of Re_{crit} would be consistent with a 106 km turbopause if either Re_T or Re_o is the relevant Reynolds number. Re_{crit} would have to be less than 1000 for Re_d and less than 400 for Re_t to be the relevant Reynolds number. None of these possibilities is unreasonable. Therefore the observed turbopause at 106 km is at least plausible by the Reynolds criterion. None of the Reynolds numbers (75) through (78) could satisfy the Reynolds criterion with any reasonable value of Re_{crit} for more than a few kilometers

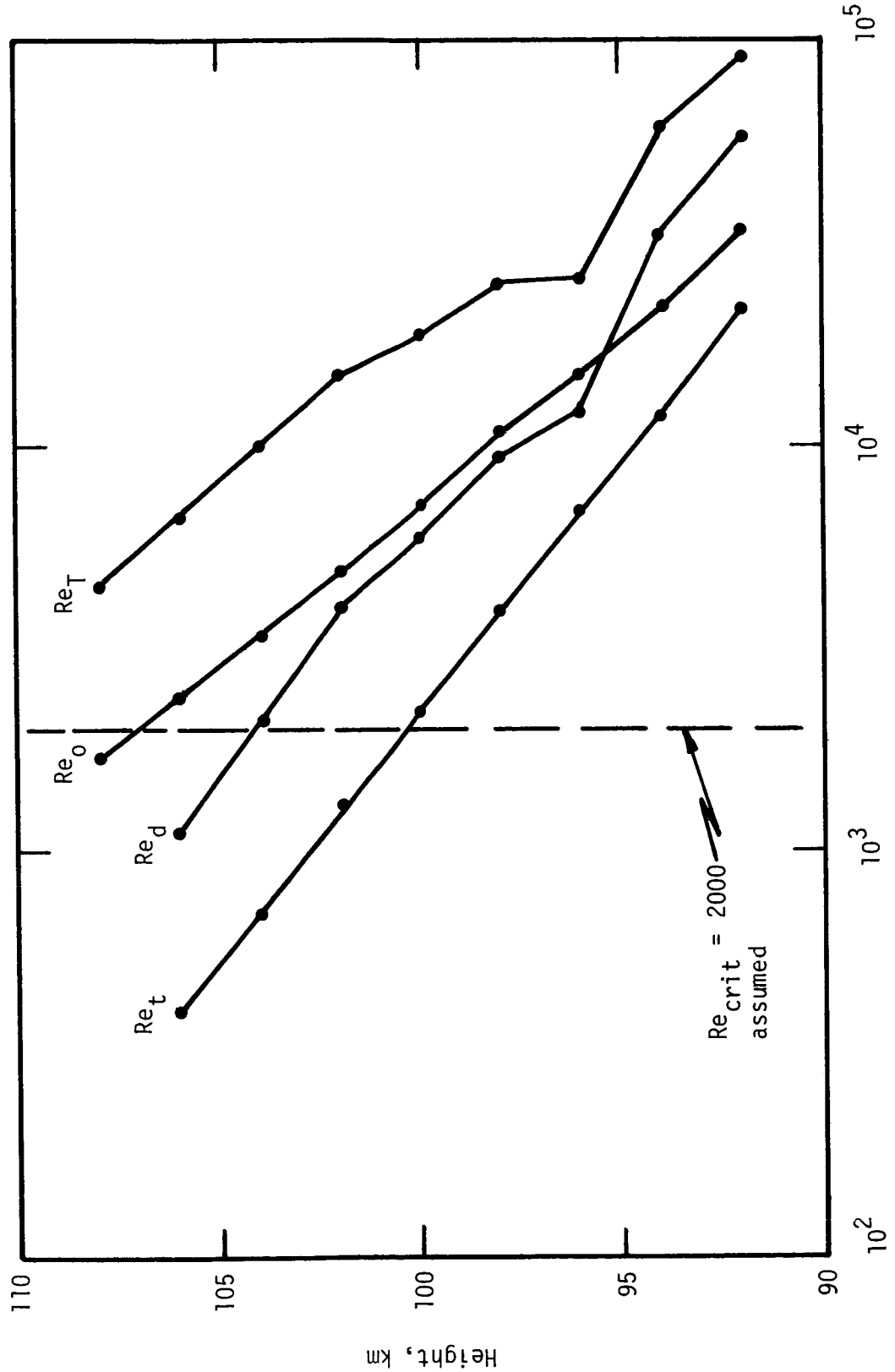

Figure 17. Calculated Reynolds Numbers versus Altitude.

above the 106 km turbopause.

Part of Hines' argument against the necessity of the Reynolds criterion is that the Reynolds number is important only at the viscous cutoff scales. Evaluation of Re^*, defined as $\frac{v^* L^*}{\eta}$, by the use of equations (49), (50) and (70) shows that $Re^* = 1$. This fact implies that the only applicable Reynolds criterion for a free atmosphere is $Re > 1$, which is the condition leading to the viscous cutoff scale. Extrapolation of the graphs in Figure 17 shows that the $Re > 1$ criterion would lead to an absolute upper limit for the turbulence cutoff altitude between 120 and 140 km. This is in agreement with a previous prediction of 120 km made by Stewart [1959], based on the same criterion.

Shear Dependent Criteria

In a free atmosphere it is stability that primarily determines whether or not turbulence is present. If the temperature gradient $\frac{\partial T}{\partial z}$ is negative and less than the adiabatic temperature gradient $-g/C_p$, the atmosphere is gravitationally unstable and the velocity gradient will almost never be so small that the turbulence will be inhibited by a low Reynolds number. When $\frac{\partial T}{\partial z} > 0$ the region is gravitationally stable and the flow will be laminar in weak velocity gradients. But if the shear is sufficiently large the region will be turbulent in spite of the gravitational stability. Several criteria have been proposed for testing the allowability of turbulence in a gravitationally stable medium.

Richardson's Criterion

Richardson's criterion [1920] is based on the assumption that if ϵ, of the energy balance equation $\epsilon_s = \epsilon_g + \epsilon$, is greater than zero, then

turbulence exists. The condition $\epsilon > 0$ is equivalent to $\epsilon_s - \epsilon_g > 0$ or $\epsilon_g/\epsilon_s < 1$. Richardson uses the approximation to equation (2)

$$\epsilon_s = \overline{v_x v_z} \frac{\partial V_x}{\partial z} = K_E \omega_s^2 \quad , \tag{79}$$

where ω_s is $\frac{\partial V_x}{\partial z}$ and K_E is given by

$$K_E = \frac{\overline{v_x v_z}}{\omega_s} \quad . \tag{80}$$

He uses for ϵ_g the form

$$\epsilon_g = K_C \omega_g^2 \tag{81}$$

with $K_C = \overline{v_z L_m}$. This is the same as equation (7). Richardson assumes that $K_E = K_C$, so the condition $\epsilon_g/\epsilon_s < 1$ is equivalent to

$$Ri = \frac{\omega_g^2}{\omega_s^2} < 1 \quad . \tag{82}$$

The Richardson criterion for the onset of turbulence is thus

$$\begin{aligned} Ri &< 1 \qquad \text{turbulent} \\ Ri &> 1 \qquad \text{laminar} \quad . \end{aligned} \tag{83}$$

Townsend's Criterion

Townsend [1957] developed a more elegant criterion for the onset of turbulence based on an analogy between turbulence and Brownian motion. For this theory the quantity ω_t defined by

$$\epsilon = \tfrac{1}{2}\left(\overline{v_x^2} + \overline{v_y^2} + \overline{v_z^2}\right)\ \omega_t \tag{84}$$

is important. Using the Brownian motion analogy, Townsend arrives at the result

$$\overline{v_z\, L_m} = \frac{\overline{v_z^2}}{2\ \omega_t} \quad . \tag{85}$$

Using this result, one may rewrite (81) as

$$\epsilon_g = \tfrac{1}{2}\, k_g\, \overline{v_z^2}\ \frac{\omega_g^2}{\omega_t} \quad , \tag{86}$$

where $k_g = 1$ for the Brownian motion analogy and is presumably close to unity for turbulence.

Equations (84) and (79) may be rewritten as

$$\epsilon = \frac{3}{2}\, k_t\, \overline{v_z^2}\ \omega_t \tag{87}$$

and

$$\epsilon_s = \frac{2}{5}\, k_s\, \overline{v_z^2}\ \omega_s \quad , \tag{88}$$

where the coefficients k_t and k_s are of order unity.

Defining the Richardson flux number as

$$Rf = \frac{\epsilon_g}{\epsilon_s} \quad , \tag{89}$$

Townsend derives the result

$$(1 - Rf)\, Rf = \frac{75}{16} \frac{k_g k_t}{k_s^2} Ri \quad . \tag{90}$$

The left side of (90) is a maximum at $Rf = \frac{1}{2}$ and at this point Ri is the critical value Ri_{crit} given by

$$Ri_{crit} = \frac{4}{75} \frac{k_s^2}{k_g k_t} \approx 0.05 \quad . \tag{91}$$

The flow will be turbulent for all $Ri < Ri_{crit}$.

Layzer's Criterion

Layzer [1961] extended the ideas of Townsend by imposing the additional restriction $\omega_t > \omega_g$. Layzer imposes this condition because he feels the situation $\epsilon_g > \epsilon$ is not likely to occur since turbulence tends to maximize the turbulent dissipation rate ϵ. For $\omega_t > \omega_g$ it is necessary that Rf satisfy the inequality

$$Rf < \frac{k_g}{k_g + 3k_t} \quad . \tag{92}$$

Combining (92) and (90), Layzer derives the condition

$$Ri < Ri_{crit} = \frac{16}{25} \left(\frac{k_s}{k_g + 3k_t} \right)^2 \approx 0.04 \tag{93}$$

for the onset of turbulence.

Generalized Richardson Criterion

Table 6 shows the observed values of several parameters which are

important in the Richardson, Townsend and Layzer criteria. From the tabulated values of Ri it is seen that the Richardson criterion would predict no turbulence in the region below 106 km. The values of ϵ_s and $\epsilon_s - \epsilon$ from Figure 6 can be used to calculate $Rf = (\epsilon_s - \epsilon)/\epsilon_s$. Table 6 shows that the Townsend relation $Ri \approx \frac{16}{75}(1 - Rf)\,Rf$ does not agree with observation. The observed values of ω_t and ω_g in Table 6 fail to satisfy $\omega_t > \omega_g$ in the altitude region below 106 km, in contradiction to the Layzer assumption. Therefore neither the Richardson, Townsend nor Layzer criterion is compatible with observation.

Apparently these theories fail because they attempt to determine if the wind shears provide sufficient energy for the existence of turbulence but use the parameters ϵ_s, ϵ_g and ϵ, which are actually power quantities associated with the eddies whose existence or non-existence is supposed to be explained by the criteria. Also the Brownian motion analogy, on which both Townsend's and Layzer's criteria depend, is probably not a good approximation for the turbulence of the upper atmosphere where the buoyancy effects are so important. The reason for the failure of Layzer's assumptions was also discussed in Chapter III.

A more appropriate energy criterion is the requirement that the buoyancy kinetic energy per unit mass $\frac{1}{2} v_b^2 = \frac{1}{4} L_b^2 \omega_g^2$ be less than the turbulent kinetic energy per unit mass $\frac{1}{2} v^2$ which can be induced by wind shears. Thus a generalized Richardson number

$$Ri^* = \frac{v_b^2}{v^2} = \frac{\frac{1}{2} L_b^2 \omega_g^2}{v^2} \tag{94}$$

can be defined. Turbulence should exist for all values of Ri^* such that

Table 6. Observed Values of Turbulence Criterion Parameters

Height (km)	ω_s (sec^{-1})	ω_g (sec^{-1})	ω_t (sec^{-1})	Ri	Rf	$\frac{16}{75}(1-Rf)Rf$
92	0.0168	0.0235	1.7×10^{-5}	1.96	0.99	0.0015
94	0.0162	0.0241	3.6×10^{-5}	2.22	0.99	0.0029
96	0.0193	0.0243	7.6×10^{-5}	1.59	0.97	0.0060
98	0.0194	0.0245	0.00016	1.60	0.94	0.011
100	0.0184	0.0245	0.00034	1.77	0.88	0.022
102	0.0188	0.0245	0.00063	1.90	0.80	0.034
104	0.0210	0.0245	0.0015	1.36	0.55	0.053
106	0.0216	0.0245	0.0031	1.29	0.09	0.018
108	0.0255	0.0245	0.0067	0.92	--	--

$Ri^* < 1$. However, v^2 may be written as $L_m^2 \omega_s^2$ by equation (48), where L_m is the mixing length. Therefore Ri^* may be put into the form

$$Ri^* = \tfrac{1}{2} \frac{L_b^2 \omega_g^2}{L_m^2 \omega_s^2} \quad . \tag{95}$$

This should be compared with a similar relation proposed by Blamont and de Jager [1961]. Table 7 lists the observed values of v^2 and the calculated values of v_b^2 and Ri^* for several altitudes. It is apparent that the condition $Ri^* < 1$ correctly predicts turbulence for all altitudes below 106 km.

In Chapter III it was pointed out that globules are influenced by the buoyancy subrange for a length of time only slightly less than $2\pi/\omega_g$. If a period $\tau_s = 2\pi/\omega_s$ is calculated using ω_s values from Table 6, it is found that the average value of τ_s between 92 and 108 km is 340 sec. This value is in good agreement with the 300 to 330 sec observed time scale τ_o of the largest eddies. Equation (58) implies that the time constant for the conversion of turbulent kinetic energy to internal energy is proportional to L_d^2/η. The period $\tau_t = 2\pi/\omega_t$ evaluated from values in Table 6 is found to satisfy the approximate relation

$$\tau_t = \frac{L_d^2}{12\,\eta} \tag{96}$$

in the height region from 92 to 108 km.

Roper [1963] has proposed that the generalized Richardson number be defined by

$$Ri_d^* = \frac{L_b^2 \omega_g^2}{L_d^2 \omega_s^2} \quad . \tag{97}$$

Table 7. Parameters for $Ri^* = v_b^2/v^2$

Height (km)	L_b (km)	v_b^2 (m^2/sec^2)	v^2 (m^2/sec^2)	Ri^*
92	0.4	44	196	0.22
94	0.4	46	185	0.25
96	0.4	47	216	0.22
98	0.61	112	159	0.70
100	0.76	173	207	0.84
102	0.76	173	303	0.57
104	0.78	182	252	0.72
106	0.88	232	222	1.05
108	1.32	525	222	2.36

Roper also derived a relation which can be expressed as

$$Ri_d^* \approx \frac{\epsilon}{10\ \eta\ \omega_s^2} \quad , \tag{98}$$

Table 8 shows the observed values of $10\ \eta\ \omega_s^2$, $\epsilon/(10\ \eta\ \omega_s^2)$ and Ri_d^*. Relation (98) is seen to produce values in reasonable agreement with the observed Ri_d^* values below the turbopause. The condition $Ri_d^* < 1$ also correctly predicts turbulence for all altitudes below 106 km, although in the lower altitudes shown in Table 8, Ri_d^* is much less than Ri^* because $L_d \gg L_m$ in this height region.

Table 8. Parameters for Ri_d^*

Height (km)	$10\ \eta\ \omega_s^2$ (m^2/sec^3)	$\frac{\epsilon}{10\ \eta\ \omega_s^2}$	Observed Ri_d^*
92	0.016	0.14	0.036
94	0.025	0.19	0.060
96	0.047	0.21	0.060
98	0.067	0.30	0.20
100	0.080	0.54	0.48
102	0.090	0.90	0.60
104	0.26	0.72	0.84
106	0.37	1.08	1.50
108	0.95	0.90	3.96

CHAPTER V

CONCLUSIONS

Turbulence exists in the upper atmosphere only to an altitude of about 106 km, as determined by examination of the globule cutoff on many chemical release clouds. The globule cutoff altitude is a good estimate of the true turbopause because the naturally occurring turbulence provides an unstable medium in which small fluctuations in the releasing of the chemical clouds lead to the globular structure. Only for releases at very uniform rates or in small concentrations would the turbulence fail to produce this globular structure up to the actual turbopause altitude. And, although globules already produced in the turbulent zone might be carried upward a short distance by such mechanisms as residual upward momentum after release or temperature buoyancy, they should not be found more than a kilometer or two above the true turbopause.

Turbulent winds determined by chemical release tracking are useful in obtaining estimates of the energy balance terms ϵ_s, ϵ_g and ϵ . Turbulent diffusion of globules at times after release $t \gtrsim 200$ sec follows a $d^2 \sim \epsilon\, t^3$ law, with the height variation of ϵ in reasonable agreement with the turbulent wind determinations of ϵ . Both ϵ_s and ϵ_g are slowly varying with altitude, ϵ_s being approximately 0.4 watts/kg in the 90 to 110 km region and ϵ_g being about 0.35 watts/kg in this height region. However, ϵ increases rapidly with altitude, varying by more than three orders of magnitude between 90 and 110 km. Data at lower altitudes indicate that ϵ continues to decrease with decreasing height, changing by an additional

three orders of magnitude or more between 90 and 30 km. Since energy balance requires that the source term ϵ_s be greater than the dissipation term ϵ, the rapid increase in ϵ is responsible for the turbopause. The turbopause altitude predicted by the observed ϵ variation is 106 km, in agreement with the observed value.

During the earliest observed phases of globule growth ($t \lesssim 150$ sec), diffusion is influenced by the buoyancy subrange, with a resulting $d^2 \sim \epsilon_g t^5$ diffusion law as predicted by Bolgiano. If more precise globule diameter measurements could be made during this phase of the globule expansion, this would provide an independent method for determining ϵ_g. However, this cannot be done at present. Only the smaller scale sizes are affected by this buoyancy subrange. During the time after release $150 \lesssim t \lesssim 200$ sec, the buoyancy subrange no longer affects globule diffusion. Expansion during this interval occurs by molecular diffusion alone. The 150 sec initial period in which buoyancy effects are observed is an appreciable fraction of the period $2\pi/\omega_g$ for harmonic oscillation of a fluid element displaced from its equilibrium point in a stably stratified atmosphere. The approximately 50 seconds of molecular diffusion corresponds closely to the theoretically predicted time scale $\sqrt{2}/\omega_g$ of the largest buoyancy subrange eddies. The maximum buoyancy subrange scale L_b varies with altitude but is approximately 0.8 km in the height range 98 to 106 km. This value can be predicted by the requirement that the characteristic buoyancy kinetic energy $\frac{1}{2} v_b^2$ must be less than the observed turbulent kinetic energy.

The decrease of L_b with decreasing altitude is responsible for the slow transition of cloud appearance from spherical globular structure to

a more general fuzzy shape. This is because the buoyancy subrange motions are more ordered than the larger scale inertial subrange motions. As L_b decreases the buoyancy subrange cannot act on the expanding cloud elements for a sufficient length of time to produce the regular spherical globules.

Diffusion at scales larger than those at which globules can usually be observed has been found by other investigators to follow a $d^2 \sim t^2$ growth law. At present it cannot be determined if this is a transition from the $d^2 \sim t^3$ globule diffusion, as would be expected from Tchen's shear turbulence theory, or whether this is merely an erroneous observation caused by difficulties in accounting for sky background on the chemical cloud observations at large scales. An alternate method, independent of sky background, for measuring large scale diffusion effects would be most useful in resolving this question. Since globule center point positions can be determined with no dependence on sky background, observations of the growth with time of the separation distance between center points of pairs of globules at approximately the same altitude would provide such a method.

All experimental evidence agrees with an energy spectrum $E(k)$ as shown in Figure 7(c). The inertial subrange, $k_o \leq k \leq k_b$, portion of E is given by equation (18) with $\alpha \approx 1$. The buoyancy subrange, $k_b \leq k \leq k^*$ ($k^* \approx k_B$, the smallest buoyancy scale), portion of E is given by (32) with θ varying with altitude and having values of 0.08 and 0.8 at 95 and 105 km respectively. Equation (18) was obtained by substituting ϵ_s for ϵ in the original non-buoyancy formulation. This alteration of (18), as well as other relations coming originally from non-buoyancy theories, is justifiable since for turbulence with no buoyancy effects $\epsilon_s = \epsilon$.

The shear and energy spectrum functions $\bar{E}(\xi)$ and $F(\xi)$ given by (24) and (25) are approximately correct in the turbulent region when only vertical, shear influenced displacements ξ are considered and the residual wind profiles are used. The slightly higher than expected exponents actually observed for the $\bar{E}$ and $\bar{F}$ power laws (≈ 0.7 and 1.5 respectively) might be an effect of the slight anisotropy of the motion field or a result of buoyancy subrange influence. Above the turbopause at 106 km, the exponents of the $\bar{E}$ and $\bar{F}$ power laws are still higher (≈ 0.8 and 1.65 respectively). Thus the $\bar{F}$ power law exponent is approaching the expected value of 2.0 for a "monochromatic" velocity profile. Hence this increase in the power law exponents is explained by the turbulence transition. Maxima in the shear spectrum function are associated with a length scale of the motion by analogy with the motion spectrum function for a "monochromatic" wind profile, which has a motion spectrum function maximum at one half wave length. Between 80 and 120 km the shear spectrum scale of both the total and residual winds follows closely the height variation of the pressure scale height. Data on the vertical scale of the winds at lower altitudes indicate a continuous exponential increase from sea level to 80 km.

The horizontal motion spectrum function $f(\delta)$ given by (29) is found to be valid in the turbulent region, with $\gamma \approx 1.5$ near the 100 km level. Considering $f(\delta)$ as a horizontal equivalent of the vertical energy spectrum function $\bar{E}(\xi)$ implies that the characteristic velocity U_o of the largest eddies is about 25 m/sec. This equivalence of $f(\delta)$ and $\bar{E}(\xi)$ is justified by the fact that $f(\delta)$, given by (28), is the definition of the energy spectrum function for isotropic homogeneous turbulence, and the observed turbulence is only slightly anisotropic. Estimates of U_o made from $\bar{E}(\xi)$ are

somewhat lower than 25 m/sec, but these determinations are complicated by a residual contribution from the total winds to the observed energy spectrum function $\bar{E}_o$, as given by (30). The proper energy spectrum function $\bar{E}(\xi)$ should involve only the turbulent winds and should have no such contribution from the larger scale prevailing, tidal or gravity wave components.

Between 80 and 140 km the observed vertical autocorrelation scale, determined by equation (45), also follows closely the height variation of the scale height. Below the turbopause the ratio of the shear spectrum scale to the vertical autocorrelation scale is approximately unity. Above the turbopause this ratio approaches 2.0, the expected value for a "monochromatic" velocity profile. The shear spectrum and vertical autocorrelation scales of the residual winds should be the same as the vertical scales of the turbulent winds. They indicate a vertical scale of about seven km for the turbulent winds near 100 km. Since the horizontal scale is about 10 km, the turbulence is made only slightly anisotropic by the strong vertical shears. According to Bolgiano's original theory, buoyancy effects could also cause anisotropy of the motion field. However, since the observed buoyancy subrange affects only the smaller scales, it apparently does not contribute to the anisotropy. An estimate of the characteristic scale L_o of the largest eddies by equation (61) yields the value 8.2 km, which is a reasonable average value of the largest vertical and horizontal scales observed.

The mixing length L_m is found to oscillate about a constant value of 0.75 km below the turbopause and then increase rapidly above this altitude. Thus $L_m \approx L_b$ in the region immediately below the turbopause.

The viscous cutoff size and time scales L^* and τ^* calculated by

equations (49) and (50) are not inconsistent with observation since scales this small cannot be observed with the resolution presently obtainable.

The spatial correlation functions $g(\xi)$ given by (51), although indicating that L_o must be of the order of six km or larger, cannot be used for accurate estimates of L_o or the dissipation length L_d. The observed rapid decorrelation in the turbulent winds is probably due to the accuracy limit to which these winds can be measured. However, this rapid decorrelation may also be an effect of the buoyancy subrange acting on the small scales. L_d can be estimated by relation (57) and is found to vary with altitude, having values of 2.9 and 0.8 km at altitudes 92 and 106 km respectively. Relations among the eddy scales L^*, L_d and L_o previously derived for isotropic non-buoyancy turbulence must be modified because of the important buoyancy effects present.

The characteristic time τ_o of the largest eddies is found to be about 300 to 330 sec by both relation (70) and by direct time correlation. Thus chemical cloud lifetimes of approximately 10 minutes allow ample time for observation of most, if not all of the turbulent spectrum. The observed value τ_o is approximately equal to the period calculated by $2\pi/\omega_s$, where ω_s is the observed magnitude of the total wind shear.

The usual Richardson, Townsend and Layzer criteria for the onset of turbulence are not succesful in explaining the observed turbulence cutoff at 106 km. These theories attempt to determine if wind shears provide sufficient energy for the existence of turbulence, but use the power quantities ϵ_s, ϵ_g and ϵ in their formulation. The generalized Richardson criterion, based on the energy requirement that $\frac{1}{2}v_b^2$ must be less than the turbulent kinetic energy per unit mass which can be produced by wind shears,

leads to a generalized Richardson number Ri^*, given by (94) or (95). The criterion $Ri^* < 1$ successfully predicts turbulence for all altitudes below 106 km. Equation (98) provides a good approximation to Ri_d^*, given by (97), in the region below the turbopause. The criterion $Ri_d^* < 1$ also successfully predicts turbulence only below 106 km.

In addition to the generalized Richardson criterion, it has been proposed that the Reynolds criterion $Re > Re_{crit}$ must be satisfied if turbulence is to exist. Uncertainties as to the proper characteristic length and velocity as well as critical value for a free atmosphere make application of the Reynolds criterion only qualitative, but reasonable estimates of these parameters show that this criterion can be satisfied at most only to a few kilometers above the 106 km turbopause. However, Hines' theoretical arguments against the necessity of a Reynolds criterion in a free atmosphere may mean that this fact is only coincidental. Possibly the only restriction on the turbulence by a Reynolds criterion is the absolute upper limit of 120 to 140 km imposed by the condition $Re > 1$.

APPENDIX A

COMPARISON OF TURBULENCE ON CHEMICAL AND METEOR TRAILS

Some early investigators [e. g. Greenhow and Neufeld, 1959a, 1960] attributed many large scale irregularities in upper atmospheric winds to turbulence. However, Hines' [1960] gravity wave theory was successful in explaining many of the properties of these large scale irregularities. Greenhow and Neufeld obtained the large scale irregular wind components by subtracting 24, 12 and eight hour period Fourier components from meteor wind data obtained over all times of day. Hines [1963] has pointed out that subtraction of only these components could still leave substantial contributions from irregular tidal components and gravity waves. Hines' gravity wave explanation of the observed properties of the large scale irregularities certainly indicates that these irregularities are not entirely turbulent motions and may contain no turbulence contribution at all. The chemical release studies reported here indicate that most, if not all of the turbulent spectrum is confined to time scales less than 300 seconds. However, irregular motions with time scales much larger than 300 seconds can not be observed with existing chemical release wind analysis methods. Therefore, the question of what, if any portion of the large scale wind irregularities is turbulence must remain unanswered at the present time.

The success of Hines' theory led others [e.g. Nawrocki and Papa, 1963 and Cote, 1962] to question whether turbulence existed or not as a natural phenomenon of the upper atmosphere. One proposal was that small

scale irregularities observed on chemical and meteor trails were the result of turbulence induced by the rocket, release mechanism or meteor in its passage through the atmosphere. Turbulence could be produced in the wake of a meteor or rocket, by a jet effect from pressurized or combustion release of chemicals in trail form or by explosive release of chemicals in point release form. The key to showing that the turbulence is not artificially produced is that each of these very different methods of producing observable trails indicates the existence of turbulence, and the turbulence so observed has almost identical characteristics in each case.

A typical bright meteor [Liller and Whipple, 1954] would have a velocity of about 6×10^4 m/sec and would release approximately 10 grams of material into the atmosphere by ablation. A typical chemical release would put from one to 40 kg of material into the atmosphere from a rocket traveling at about 10^3 m/sec. If all of the kinetic energy of the released material were available for the production of turbulence, this would amount to something of the order of 10^6 or 10^7 joules in either case. For a chemical or meteor trail released over a 20 km length and having an initial cross section of 100 m^2, this would represent on the order of 1 joule/m^3. If the value 10^{-6} kg/m^3 is taken as a typical ambient density at the altitude of release, this would be about 10^6 joules/kg of atmosphere, corresponding to a turbulent velocity of about 10^3 m/sec. Since the observed turbulent velocities are of the order of 10 m/sec, only about one hundredth of the total energy is thus available for the production of turbulent winds.

If turbulence is produced by the ejection mechanism, rocket or meteor, the meteor would represent a small mass, high velocity source, and the rocket or release mechanism would represent a large mass, low

velocity source. Explosive release of chemicals would provide yet another type of energy source for the production of turbulence. It would be expected that these drastically different characteristics in the source would produce observable differences in the resultant turbulence. However, calculations of the turbulence power ϵ, discussed in Chapter I, from both meteor and chemical trails as well as explosive releases all show reasonable agreement with one another [Greenhow, 1959, Blamont and de Jager, 1961, Roper, 1963 and Noel, 1963]. The observed globule cutoff altitude is also much the same for both the trail and explosive chemical releases analyzed during this work. The globule cutoff altitude reported here also agrees well with that observed by other investigators [e.g. Blamont and de Jager, 1961], using very different release mechanisms and launch vehicles. With these observed similarities, it seems doubtful that the observed turbulence is artificially produced.

As further proof that the turbulence is a naturally occurring ambient phenomenon, a calculation can be made of the time variation of the turbulent velocity that could be induced in the wake of a passing rocket or meteor or as a jet effect from a passing pressurized or combustion releasing mechanism. Schlichting [1960] has shown that the maximum turbulent velocity present at a time t after the passage of a wake producing body is given by

$$v = \frac{C_1}{t^{2/3}} \quad , \tag{99}$$

and after the passage of a turbulence producing jet by

$$v = \frac{C_2}{t} \quad . \tag{100}$$

For the choice of C_1 and C_2 values such that both (99) and (100) yield $v = 15$ m/sec at $t = 100$ seconds after the passage of the rocket or meteor, Table 9 shows values of v at various times t. Table 9 also shows the average observed turbulent velocities for one rocket released cloud. Although these observed turbulent velocities remain constant with time, they are somewhat lower than the usual 15 m/sec observed. Even so, the predicted jet and wake turbulent velocities are too small to agree well with the observed values at the latest time. Usually turbulent velocities are not calculated during the first 90 seconds after release of the cloud, because of the velocity deviations which might occur during this period. However, any early anomalous velocity deviations are certainly less than about 20 m/sec, as has been shown by determinations of winds during this period from a few chemical releases. Therefore Table 9 shows that the jet and wake turbulent velocities required at $t = 10$ sec are entirely too large. Thus the required variation of the turbulent velocity produced in the wake of either a meteor or rocket or the jet of a release mechanism is entirely incompatible with the observed turbulent velocities.

The observed energy dissipation rate in the turbulence also leads to the conclusion that the turbulence is an ambient phenomenon. If the rocket, release mechanism or meteor induced an initial turbulent velocity v_o, and there were no ambient source for the maintenance of the turbulence, then at a time t after the release, the turbulent velocity v would be given by

$$\tfrac{1}{2}(v_o^2 - v^2) = \epsilon_s t \quad , \tag{101}$$

where $\epsilon_s = \epsilon_g + \epsilon$ is the observed total energy dissipation rate per unit

Table 9. Predicted Jet and Wake Turbulent Velocities and Observed Turbulent Velocities

t (sec)	v (m/sec)		
	jet	wake	observed
10	150	70	(< 20)
100	≅15	≅15	9.7
250	6.0	8.1	10.7
440	3.4	5.5	9.9
620	2.4	4.5	11.2

mass of atmosphere. Figure 6 of Chapter I shows that $\epsilon_s \approx 0.4\ m^2/sec^3$. Solving (101) for v^2 yields

$$v^2 = v_o^2 - 2\,\epsilon_s\,t \quad . \tag{102}$$

If it is required that v = 20 m/sec at t = 100 sec, then the observed value of ϵ_s implies that v would go to zero by the time t = 600 sec, in obvious disagreement with the observed turbulent velocities in Table 9. Since the early anomalous velocity deviations are damped out during approximately the first 90 seconds after release, equation (102) implies that the actual turbulent velocity induced by the rocket, release mechanism or meteor must be less than 10 m/sec, in aggrement with observation.

APPENDIX B

DERIVATION OF EQUATION (67)

The virial theorem states that

$$\overline{T} = -\tfrac{1}{2}\,\overline{\underline{F}\cdot\underline{r}} \quad , \tag{103}$$

where T is the kinetic energy of a single body system and $\underline{F}$ is the force acting on the system located by the position vector $\underline{r}$. Considering a fluid element in the buoyancy subrange as a harmonic oscillator acted on by a force

$$\underline{F} = -k\,\underline{r} = -m\,\omega_g^2\,\underline{r} \quad , \tag{104}$$

then the average kinetic energy per unit mass $\frac{1}{2}\,v_b^2$ is

$$\tfrac{1}{2}\,v_b^2 = \frac{\overline{T}}{m} = \tfrac{1}{2}\,\omega_g^2\,\overline{r^2} \quad . \tag{105}$$

If the amplitude of oscillation is taken to be the largest buoyancy scale L_b, then

$$\begin{aligned}
\tfrac{1}{2}\,v_b^2 &= \frac{1}{4\pi}\,\omega_g^2\,L_b^2 \int_0^{2\pi/\omega_g} \sin^2(\omega_g\,t + \alpha)\;\omega_g\,dt \\
&= \frac{1}{4\pi}\,\omega_g^2\,L_b^2 \int_0^{2\pi} \sin^2\theta\,d\theta \\
&= \tfrac{1}{4}\,L_b^2\,\omega_g^2 \quad ,
\end{aligned} \tag{106}$$

which is the result stated in equation (67).

Another result of the virial theorem is that for a single body system acted on by a power law force $F \sim r^n$

$$\overline{T} = \frac{n+1}{2} \overline{V} \quad , \tag{107}$$

where V is the potential energy of the system. Thus for an harmonic oscillator $\overline{T} = \overline{V}$, and the requirement that the buoyancy kinetic energy per unit mass be less than $\frac{1}{2} v^2$ is equivalent to imposing the same condition on the buoyancy potential energy per unit mass.

BIBLIOGRAPHY

1. Batchelor, G. K., "Kolmogoroff's Theory of Locally Isotropic Turbulence", Proceedings of the Cambridge Philosophical Society, 43, 533-559, 1947

2. Batchelor, G. K., "The Application of the Similarity Theory of Turbulence to Atmospheric Diffusion", Quarterly Journal of the Royal Meteorological Society, 76, 133-146, 1950

3. Batchelor, G. K., The Theory of Homogeneous Turbulence , Cambridge University Press, 1953

4. Blamont, J. E. and C. de Jager, "Upper Atmospheric Turbulence Near the 100 Km Level", Annales de Geophysique, 17, 134-144, 1961

5. Bolgiano, Jr., R., "Turbulent Spectra in A Stably Stratified Atmosphere", Journal of Geophysical Research, 64, 2226-2229, 1959

6. Cote, O., "On the Question of Turbulence in the Upper Atmosphere", (NASA Report), Geophysics Corporation of America Technical Report no. 62-12-N, 1962

7. Cote, O., "Turbulent Diffusion of Sodium Vapor Trails in the Upper Atmosphere", Geophysics Corporation of America Technical Report no. 65-5-N, 1965

8. Greenhow, J. S., "Eddy Diffusion and its Effect on Meteor Trails", Journal of Geophysical Research, 64, 2208-2209, 1959

9. Greenhow, J. S. and E. L. Neufeld, "Measurements of Turbulence in the Upper Atmosphere", Proceedings of the Physical Society (London), 74, 1-10, 1959a

10. Greenhow, J. S. and E. L. Neufeld, "Measurements of Turbulence in the 80 to 100 Km Region from the Radio Observations of Meteors", Journal of Geophysical Research, 64, 2129-2133, 1959b

11. Greenhow, J. S. and E. L. Neufeld, "Large Scale Irregularities in High Altitude Winds", Proceedings of the Physical Society (London), 75, 228-234, 1960

12. Hines, C. O., "Internal Atmospheric Gravity Waves at Ionospheric Heights", Canadian Journal of Physics, 38, 1441-1481, 1960

13. Hines, C. O., "The Upper Atmosphere in Motion", Quarterly Journal of the Royal Meteorological Society (London), 89, 1-42, 1963

Bibliography (Cont'd.)

14. Justus, C. G., H. D. Edwards and R. N. Fuller, "Analysis Techniques for Determining Mass Motions in the Upper Atmosphere from Chemical Releases", Scientific Report AFCRL-64-187, 1964a

15. Justus, C. G., H. D. Edwards and R. N. Fuller, "A Method Employing Star Backgrounds for Improving the Accuracy of the Location of Clouds or Objects in Space", Photogrammetric Engineering , 30, 594-607, 1964b

16. Kolmogoroff, A. N., "The Local Structure of Turbulence in an Incompressible Viscous Fluid for very Large Reynolds Numbers", Comptes Rendus (Doklady) Akademiia Nauk SSSR, 30, 301-305, 1941a

17. Kolmogoroff, A. N., "Dissipation of Energy in the Locally Isotropic Turbulence", Comptes Rendus (Doklady) Akademiia Nauk SSSR, 32, 16-18, 1941b

18. Lamb, H., Hydrodynamics, Dover Publications, 1945

19. Layzer, D., "The Turbulence Criterion in Stably Stratified Shear Flow and the Origin of Sporadic E", unpublished notes, 1961. See also reference 23 below.

20. Lettau, H. H., "Dissipation of Energy by Turbulence", Journal of Meteorology, 18, 125-126, 1961

21. Liller, W. and F. L. Whipple, "High Altitude Winds by Meteor Train Photography", Special Supplement to the Journal of Atmosphere and Terrestrial Physics, 1, 112-130, 1954

22. Lin, C. C., "On a Theory of Dispersion by Continuous Movements", I and II, Proceedings of the National Academy of Sciences, 46, 566-570 and 1147-1150, 1960

23. Nawrocki, P. J. and R. J. Papa, Atmospheric Processes, Prentice-Hall, 1963

24. Noel, T. M., "A Measurement of Turbulence Power and Small Eddy Scales near 105 Kilometers", Journal of Geophysical Research, 68, 2862-2863, 1963

25. Richardson, L. F., "The Supply of Energy from and to Atmospheric Eddies", Proceedings of the Royal Society (London), A97, 354-373, 1920

26. Roper, R. G., "Atmospheric Turbulence in the Meteor Region", University of Adelaide (Australia) thesis, 1963

27. Rosenberg, N. W. And C. G. Justus, "Space and Time Correlations of Ionospheric Winds", presented at the American Geophysical Union meeting 19-22 April, Washington, D. C., and to be published, 1965

Bibliography (Cont'd.)

28. Schlichting, H., Boundary Layer Theory, McGraw-Hill, 1960

29. Stewart, R. W., "Transactions of the International Symposium on Fluid Mechanics in the Ionosphere", Journal of Geophysical Research, 64, 2084, 1959

30. Taylor, G. I., "Statistical Theory of Turbulence", Proceedings of the Royal Society (London), A151, 421-478, 1935

31. Tchen, C. M., "Transport Processes as Foundations of the Heisenberg and Obukhoff Theories of Turbulence", Physical Review, 93, 4-14, 1954

32. Tchen, C. M., "Diffusion of Particles in Turbulent Flow", Advances in Geophysics, 6, 165-173, 1961

33. Townsend, A. A., The Structure of Turbulent Shear Flow, Cambridge University Press, 1956

34. Townsend, A. A., "Turbulent Flow in a Stably Stratified Atmosphere", Journal of Fluid Mechanics, 3, 361-372, 1957

35. Webb, W. L., "Scale of Stratospheric Detail Structure", U. S. Army Report no. N64-20309, 1964

36. Zimmerman, S. P., "Upper Atmospheric Turbulence Near the 100 Km Level", Annales de Geophysique, 18, 116-117, 1962

37. Zimmerman, S. P., "Small-Scale Wind Structure above 100 Kilometers", Journal of Geophysical Research, 69, 784-785, 1964

VITA

Carl Gerald (Jere) Justus was born October 2, 1939 in Atlanta, Georgia. His parents are Luther Carl and Lorena Daniel Justus. He received his elementary and secondary education in the public schools of Fulton County, Georgia. In 1961 he received the degree of Bachelor of Science in Physics from the Georgia Institute of Technology, and was awarded the Master of Science in Physics from the same school in 1963.

The writer has been employed since 1961 as a graduate research assistant with the Space Sciences Laboratory of Georgia Tech. His publications include references 14, 15 and 27 in the Bibliography, as well as the following:

"Upper Atmospheric Wind Measurements Determined from Twelve Rocket Experiments", Journal of Geophysical Research, 68, 3021-3032, 1963, (Co-authors H. D. Edwards, M. M. Cooksey, R. N. Fuller and D. L. Albritton)

"Evening Twilight Winds from 68 to 140 Kilometers for May 21, 1963", Journal of Geophysical Research, 68, 6062-6063, 1963, (Co-authors H. D. Edwards and D. C. Kurts)

"Turbulence in the Upper Atmosphere", Air Force Cambridge Research Laboratory Final Report No. AFCRL-64-700, 1964, (Co-author H. D. Edwards).

The writer is a member of the Tau Beta Pi, Sigma Pi Sigma and Phi Eta Sigma student honorary societies, as well as the Sigma Xi professional research society. He is also a student member of the American Geophysical Union.

In 1963 the writer was married to the former Miss Helen Earline Hudson of Hapeville, Georgia.